UNIVERSITY OF CALIFORNIA

SANTA CRUZ

Luminosity and Energy Studies at a Future Linear Collider with an Emphasis on Biases in the Luminosity-Weighted Center-Of-Mass Energy

A thesis submitted in partial satisfaction
of the requirements for the degree of

MASTER OF SCIENCE

in

PHYSICS

By

Arik Florimonte

December 2005

The Thesis of Arik Florimonte
is approved:

_____
Professor Clemens A. Heusch, Chair

_____
Dr. Michael B. Woods

_____
Professor Robert P. Johnson

_____
Lisa C. Sloan
Vice Provost and Dean of Graduate Studies

Table of Contents

List of Figures

List of Tables

Abstract

I present results from luminosity and energy studies at a future Linear Collider with an emphasis on biases that arise when determining the luminosity-weighted center-of-mass energy. I compare e^+e^- and e^-e^- modes of operation and consider both NLC and TESLA beam parameters at a center-of-mass energy of 500GeV. Realistic colliding beam distributions are used, which include dynamic effects of the beam transport from the Damping Rings to the Interaction Point. Effects from beam energy spread, beamsstrahlung, correlated beam parameters, and a transverse y-z kink instability are considered. A study using Bhabha acolinearity measurements to resolve center-of-mass energy biases is also described.

1 Introduction

I perform simulations of collisions at the Linear Collider (LC) Interaction Point. I compare e^+e^- and e^-e^- modes of operation and consider both NLC and TESLA beam parameter specifications at a center-of-mass energy of 500GeV. (These energies are a step along the way to the goal of a 1-TeV linear collider.) Central to this work is development of an understanding of the biases that arise in determining the luminosity-weighted center-of-mass energy, E_{CM}^{lum-wt}. As in previous studies[1], I utilize the realistic colliding beam distributions that were generated for the TRC study[2], which compared the performance for competing Linear Collider designs. The TRC files were used to create the *electron.ini* and *positron.ini* files, which are then used as input into the GUINEA PIG[3] (GP) simulation tool for beam-beam collisions. In addition, I have also examined an additional set of *electron.ini* and *positron.ini* files which were generated in a study[4] of alternate simulation parameters designed to achieve narrow energy spread for NLC-500.

Energy and luminosity are the two most important parameters for determining the utility of a linear collider in probing new areas of particle physics. An electron-positron linear collider also has the advantage of a well-defined initial state. However, beam energy spread, beamsstrahlung, and beam disruption angles contribute to the loss of precision of the beam parameters.

While the beam energy spectrometers can be counted upon to measure $\langle E \rangle$, the luminosity can vary dependent upon the incoming beam parameters. As a result, $\langle E_{CM}^{lum-wt} \rangle$ can differ from $\langle E \rangle$. The difference of these lead to a center-of-mass energy bias, E_{CM}^{bias} as described in the next section. This bias arises due to beam energy spread, energy-z correlations within the bunch, and a y-z kink instability[5].

1.1 Motivation

The Standard Model of particle physics gives a precise description of the interactions of quarks and leptons, and its predictions have been confirmed repeatedly by experiment. However, phenomena have been observed, both in high energy physics and astrophysics which the standard model cannot explain. One of the key ingredients in probing these further mysteries is to unearth the details of the Higgs boson.

The Higgs boson is a theoretical mechanism, a particle whose interactions are theorized to endow each elementary particle its mass. If it exists, precise measurement of the Higgs boson mass will require a TeV-scale electron-positron linear collider. In addition, it is speculated the 1-TeV scale will be fertile ground for discovery[6], and among the many future experiments will be included measurement of the mass of the top quark.

In order to measure the top quark and/or Higgs boson mass with precision, we need to determine the luminosity-weighted center of mass energy, $\langle E_{CM}^{lum-wt} \rangle$, to an accuracy of 200 parts-per-million (ppm) or better[7]. Additional studies requiring precise energy measurements might include improving the precision of the existing W mass measurement or performing a very precise A_{LR} measurement in a Giga-Z program[1]. These measurements would require knowledge of $\langle E_{CM}^{lum-wt} \rangle$ to an accuracy of 50 ppm or better[7].

The Bhabha acolinearity method[8] proposes to use beam energy spectrometers to measure the average incident energies per bunch, and use Bhabha acolinearity calculations to infer the effects of beam energy spread and beamsstrahlung. Other possible methods include the analysis of radiative return events and other physics results to monitor the luminosity spectrum:

$$e^+e^- \rightarrow Z\gamma \rightarrow f\bar{f}\gamma$$
$$e^+e^- \rightarrow Z^+Z^-$$
$$e^+e^- \rightarrow W^+W^-$$

The rms energy spread for NLC (TESLA) is 3000 (1000) ppm, far less precise than the 50-200 ppm precision we seek. Therefore, we need to be

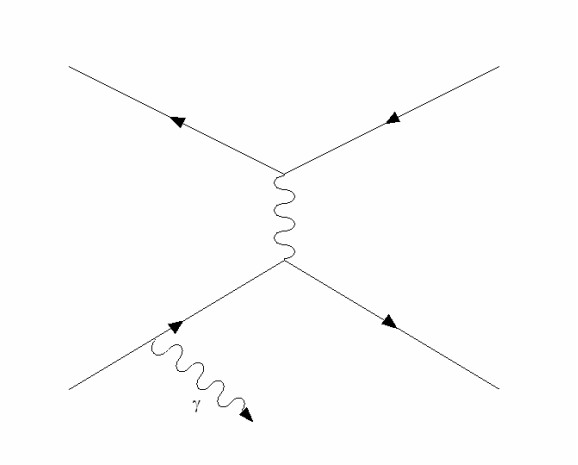

Figure 1- Initial State Radiation: the emission of a photon by one of the incoming particles prior to collision. This process can be predicted accurately using QED.

able to determine the effects of energy spread and beamsstrahlung to a high degree of accuracy.

The effects of both beamsstrahlung and initial state radiation (ISR) are potentially larger than those of energy spread. Energy spread due to beamsstrahlung is expected to be in the range of 1-3%[9], while energy spread due to ISR is calculated to be 11.9%[10] at 500 GeV. However, it is assumed that beamsstrahlung can be understood to high precision using the Bhabha acolinearity technique. ISR can be predicted accurately by applying QED.

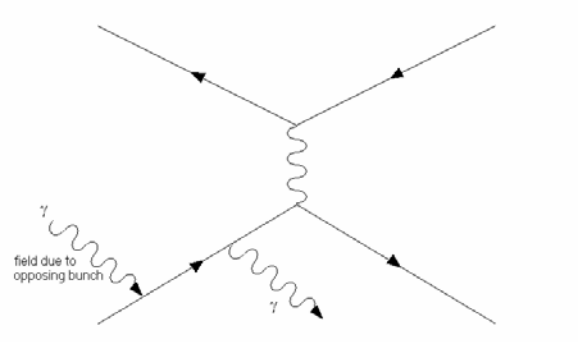

Figure 2- Beamsstrahlung: an incoming particle is deflected by the field due to the opposing bunch, resulting in the emission of a photon prior to collision. This process can be not predicted accurately using QED because of uncertainties in the field due to the opposing bunch.

1.2 Methodology

The currently favored analysis technique to determine E_{CM}^{lum-wt} is to use beam energy spectrometers to measure the average incident energies per bunch, and use Bhabha acolinearity calculations to infer the effects of beam energy spread and beamsstrahlung. In the simulation study here, the energy values from the TRC files take the place of spectrometer measurements.

Initial studies centered on understanding the luminosity spectrum without considering beamsstrahlung or Initial State Radiation (ISR). For both e^+e^- and e^-e^- interactions, simulations were run to determine the both luminosity spectrum and resulting values for $E_{CM}^{bias}\Big|_{BSoff}$. A relatively large value for $E_{CM}^{bias}\Big|_{BSoff}$ was found and attributed to a correlation between the energy of a particle and its longitudinal position in the bunch. The electron bunch can be imagined as a long ribbon a few nanometers thick, several hundred nanometers wide and a few hundred microns long. Small distortions in this beam "ribbon" are present due to wakefield effects in the incoming distributions and beam-beam interaction effects. These distortions are larger for the tail end of the bunch, resulting in lower luminosity in the tail of the bunch and leading to these Energy-z correlations.

In addition, I examined the effects on the luminosity spectrum and $E_{CM}^{bias}\Big|_{BSoff}$ for both optimized collisions (when the beams are aligned to collide perfectly) and imperfect collisions. It was found that $E_{CM}^{bias}\Big|_{BSoff}$ for all three accelerator designs considered is sensitive to minor offsets or dispersions in the colliding beams.

Subsequently, I expanded the study of luminosity spectrum to include the effects of beamsstrahlung. I examined the luminosity spectrum and resulting $E_{CM}^{bias}\Big|_{BSon}$, again for both e^+e^- and e^-e^- interactions, and for both optimized and imperfect collisions.

The resulting $E_{CM}^{bias}\big|_{BSon}$ was found to be significantly larger than $E_{CM}^{bias}\big|_{BSoff}$, and the sensitivity to imperfection collisions was exacerbated as well. Finally, I undertook a study to illustrate why the Bhabha method cannot resolve this bias.

1.3 Parameters for the Linear Collider

In 2004, the International Committee for Future Accelerators (ICFA) formed the International Technology Recommendation Panel (ITRP) to evaluate accelerator technologies and to recommend a single choice for the next linear collider. The goal of the committee was to unify the High Energy community behind one technology choice and thereby apply the available (financial) resources more efficiently. The primary candidates considered were the NLC and TESLA designs (refer to Table 1 below for an enumeration of the beam parameters for each design). The NLC uses 11.4 GHz room-temperature copper RF accelerating cavities, while the TESLA design used superconducting RF cavities at 1.3 GHz.

Among the issues considered by the committee was the achievable precision of energy measurements. Notably, energy stability and energy precision, as well as understanding of the luminosity spectrum, would need to be better than 0.1%[5] in order to carry out the planned physics program. While acknowledging the advantages for each technology, the ITRP issued its final recommendation in favor of the TESLA technology.

Table 1 - NLC and TESLA beam parameters for a 500-GeV linear collider

Beam Parameter	NLC-500	TESLA-500
Beam Energy	250 GeV	250 GeV
Repetition Rate	120 Hz	5 Hz
Bunch Charge (N)	$0.75 \cdot 10^{10}$	$2.0 \cdot 10^{10}$
Bunches per RF pulse	192	2820
Bunch spacing	1.4 ns	337 ns
Bunches per second (f_{rep})	$2.30 \cdot 10^{4}$	$1.41 \cdot 10^{4}$
$\gamma\varepsilon_x$, $\gamma\varepsilon_y$	$(360,4.0) \cdot 10^{-8}$ mrad	$(1000,3.0) \cdot 10^{-8}$ mrad
β_x, β_y	(8, 0.11) mm	(14, 0.40) mm
σ_x, σ_y	(243, 3.0) nm	(554, 5.0) nm
σ_z	110 μm	300 μm
σ_E/E electrons	0.30%	0.14%
σ_E/E positrons	0.30%	0.07%
Geometric Luminosity (L_0)	$1.4 \cdot 10^{34}/cm^2 \cdot s$	$1.6 \cdot 10^{34}/cm^2 \cdot s$
Pinch Enhancement (H_D)	e^+e^-: 1.5; e^-e^-: 0.4	e^+e^-: 2.1; e^-e^-: 0.3
Effective Luminosity (L)	e^+e^-: $2.1 \cdot 10^{34}/cm^2 \cdot s$ e^-e^-: $0.56 \cdot 10^{34}/cm^2 \cdot s$	e^+e^-: $2.9 \cdot 10^{34}/cm^2 \cdot s$ e^-e^-: $0.42 \cdot 10^{34}/cm^2 \cdot s$

A summary of the NLC and TESLA colliding beam parameters is given in Table 1, where

$\gamma\varepsilon_x$, $\gamma\varepsilon_y$:	emittance
β_x, β_y:	beam beta function at IP
σ_x, σ_y, σ_z	beam sizes in each dimension
σ_E/E	electron energy spread
L_0	Geometric Luminosity, given by:

$$L_0 = \frac{f_{\text{rep}} N^2}{4\pi\sigma_x\sigma_y}$$

Beam-beam focusing effects can result in a pinch effect, enhancing luminosity for e^+e^- collisions. For e^-e^- collisions, there is an anti-pinch resulting in reduced luminosity. The effective luminosity is given by:

$$L = L_O \cdot H_D$$

2 Beam Simulations

To simulate positron-electron and electron-electron collisions, realistic beam distributions are used, using parameters for both TESLA and NLC. These distributions were generated for the TRC Study[2], using full simulation of the transport of the beam from Damping Rings to the Interaction Point (IP). Many previous IP collision studies assumed Gaussian distributions with no correlations between beam parameters. The beam distributions used here are more realistic, and include effects from Linac wakefields and beam component misalignments. The resulting beam distributions are fed into the GUINEA PIG (GP)[3] program to simulate the collision at the IP. The output of simulations is analyzed using Matlab.

2.1 Incoming Beam Distributions at the Interaction Point

The TRC Study generated incoming beam distributions using the parameters listed in Table 1. It applied a set of misalignment errors to the Linac and then used Linac steering and modeling of IP feedback to optimize the beam transport, center the colliding beams, and optimize luminosity. The collision parameters utilized for both

TESLA and NLC are delineated in Table 1. Multiple file sets are were used, with each file set having a different set of initial misalignments. As a result, the different output files effectively simulate several different machines.

These results were used to create the *electron.ini* and *positron.ini* files, which are used as input for GP simulations of collisions. Each file contains six parameters: the energy, x- and y- angle, and x, y, and z coordinates of each particle of an incoming bunch. In this study, I examined thirteen sets of these input files: six different sets each for NLC-500 and TESLA-500 (corresponding to different beam component misalignments and IP collision optimization), as well as one additional set of files which were generated in a study[4] of alternate phase BNS configuration designed to narrow energy spread for NLC-500 (referred to hereafter as NLC′). This alternate phase BNS achieves reduced overall energy spread using a different optimization of linac rf phasing and bunch compression. The result is lower energy spread in the core of the bunch at the expense of greater energy spread in the head and the tail of the bunch (refer to Figure 3 on page 13 to see this graphically).

2.2 Simulation of the Colliding Beam using Guinea Pig

GUINEA PIG (GP) is a tool for simulating collisions at the Interaction Point. One can use GP by modifying built-in beam parameters to produce uncorrelated Gaussian incoming beam distributions, or choose to specify the beams exactly. In this study, I

specified the beams using the external *electron.ini* and *positron.ini* files, described above, as input into GP. In addition, GP takes as input the file *acc.dat* (see Appendix A.1) which contains the accelerator specifications (noted in Table 1).

Using the features built into GP, I varied certain collision parameters, such as vertical and horizontal offset, vertical dispersion, and the offset of the vertical and horizontal waist. (The waist is the longitudinal point where the beam is focused; optimally the point of best focus for both horizontal and vertical waist occurs in the z=0 plane.) In addition, I was able to specify those aspects of the collision that I wished to study (or ignore), such as beamsstrahlung or initial state radiation, by selection of a flag within *acc.dat*.

When each simulation is completed, GP generates output of outgoing beam distributions, saved as files: *beam1.dat* and *beam2.dat* contain outgoing beam distributions, and *lumi.ee.out* contains parameters of only those particles which generate luminosity.

2.3 Analysis of Results using Matlab

Nearly all of the simulations were performed using Matlab, a powerful mathematical software package. Within Matlab, GP was called using the "DOS" command. This allowed customization and automation of simulation runs. From within Matlab,

acc.dat was created with the parameters corresponding to the accelerator technology being studied. Then, the desired *electron.ini* file could be copied to the correct location so as to be utilized when GP was called. Finally, upon completion of the GP simulation, the output files from GP could be automatically saved to a specified filename or directory.

An additional advantage of using Matlab was that a large number of simulations could be repeated using a single script file. In practice, these runs were automated by setting up a loop to step through values of a variable being studied (e.g. vertical offset. Refer to Appendix A.5 for an example of the program), or to step through the indices of the 13 sets of *electron.ini* and *positron.ini* files. The output files at the end of each GP simulation were then renamed to something descriptive for later analysis.

Finally, Matlab was used to generate plots of the variables being studied. This could be done at the end of a single simulation run, for example in order to examine the Energy-Z correlation in the incoming beams, or after the fact by loading in the previously saved values into an array, for example when performing a scan of vertical offset.

3 Results

To precisely measure the top quark and/or Higgs boson mass, we need to determine the luminosity-weighted center of mass energy, $\langle E_{CM}^{lum-wt} \rangle$, to an accuracy of 200 ppm or better, and improved W-mass scans require 50 ppm or better.

3.1 E_{CM}^{bias} in the absence of beamsstrahlung

GP is run with the flags for initial state radiation and beamsstrahlung switched off. $E_{CM}^{bias}\Big|_{BSoff}$ is defined as follows:

$$E_{CM}^{bias}\Big|_{BSoff} = \left\langle E_{CM}^{lum-wt} \right\rangle - \left(\left\langle E_{1}^{ini} \right\rangle + \left\langle E_{2}^{ini} \right\rangle \right) \qquad (1)$$

where:

$$\left\langle E_{CM}^{lum-wt} \right\rangle = \left\langle E_{1}^{lum-wt} \right\rangle + \left\langle E_{2}^{lum-wt} \right\rangle$$

$\langle E_{1,2}^{ini} \rangle$ are the average energies of the incoming beams, calculated from the input files *electron.ini* and *positron.ini*. $\langle E_{1,2}^{lum-wt} \rangle$ are the average energies of the colliding particles that create luminosity, taken from the GP output file *lumi.ee.out*.

First I examine the incoming beam energy-z distributions for NLC-500, TESLA-500, and NLC′-500 (Note the TESLA graphs in the middle row are on a larger distance scale). This is shown in Figure 3. There is a clear energy-z correlation, particularly

for the NLC/NLC′ parameters. The energy spread and correlation are greater for NLC than for TESLA because of larger wakefield effects in the Linac due to the higher rf frequency and correspondingly smaller aperture.

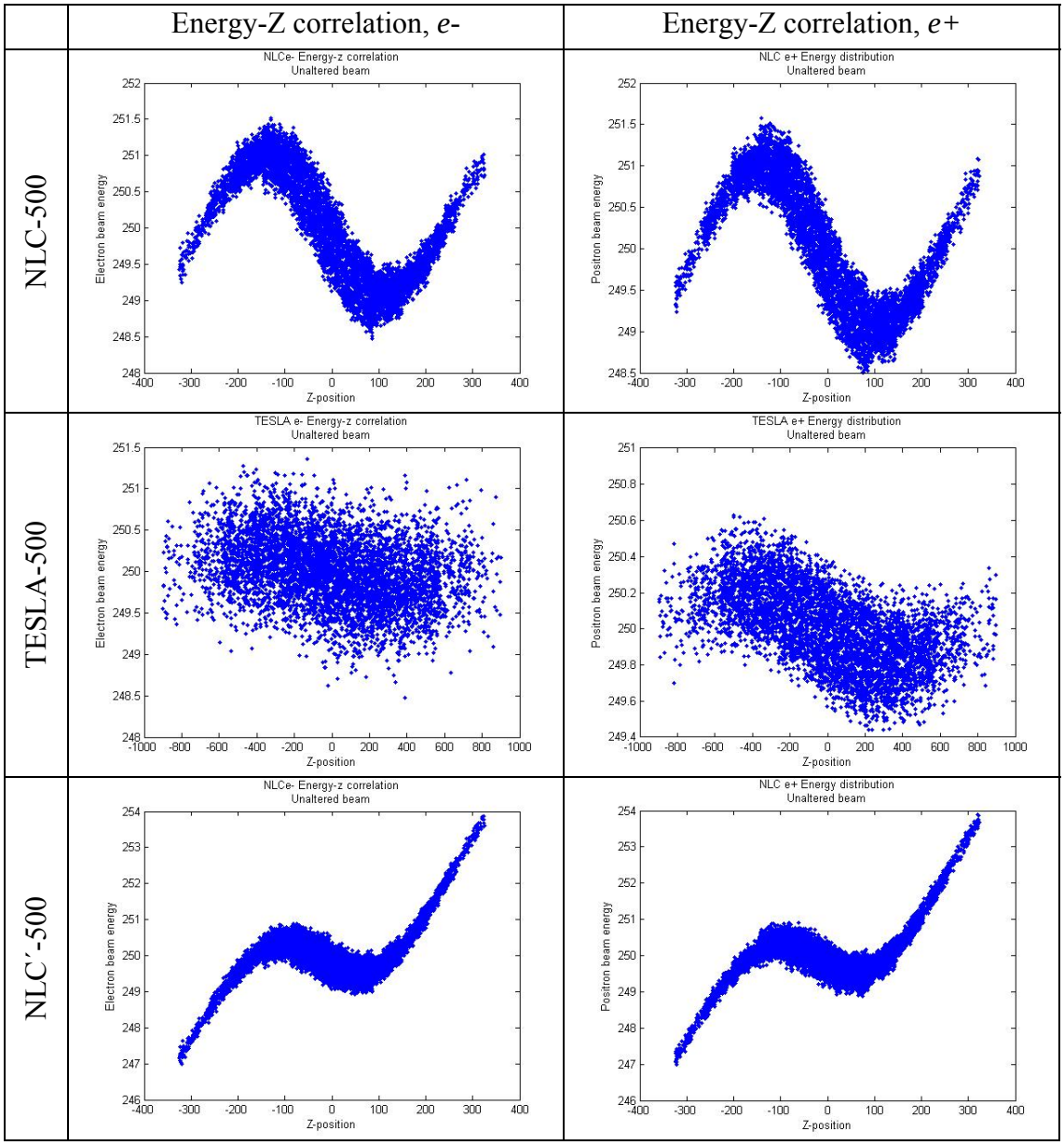

Figure 3 - Energy-z distributions for incoming beams for three LC parameter sets (NLC, TESLA, NLC′). Electron distributions are plotted in the left columns, and positron distributions are plotted in the right column.

3.1.1 Effects in e^+e^- collisions

The GP simulation is used to study e^+e^- collisions for the incoming beam distributions shown in Figure 3. Results for the E_{CM}^{lum-wt} distributions are shown in Figure 5. The first column in this figure shows examples of the incoming beam distributions for all three different accelerator configurations: NLC, TESLA, and NLC'. The second column shows the corresponding E_{CM}^{lum-wt} distributions. Each plot in the second column also has overlaid upon it a graph of what this distribution would look like if the Energy-z correlation were removed, labeled "Random E". To remove the energy-z correlation, the E-distribution in the *electron.ini* and *positron.ini* input files was unchanged but was re-ordered randomly among the ten-to-fifteen thousand particles in the files (refer to Appendix A.6).

Note the obvious asymmetry in the E_{CM}^{lum-wt} results for NLC-500. This results from the energy-z correlation combined with a kink instability. The head of each bunch has higher energy than the tail (see Figure 4), so the head-head collisions generate the higher energy portion of the distribution, the head-tail the central peak, and the tail-tail the lower energy end. Distortions, both from the initial beam and due to beam-beam effects, can grow during the collision and the resultant kink instability tends to disperse the tails and result in lower luminosity for tail-tail collisions.

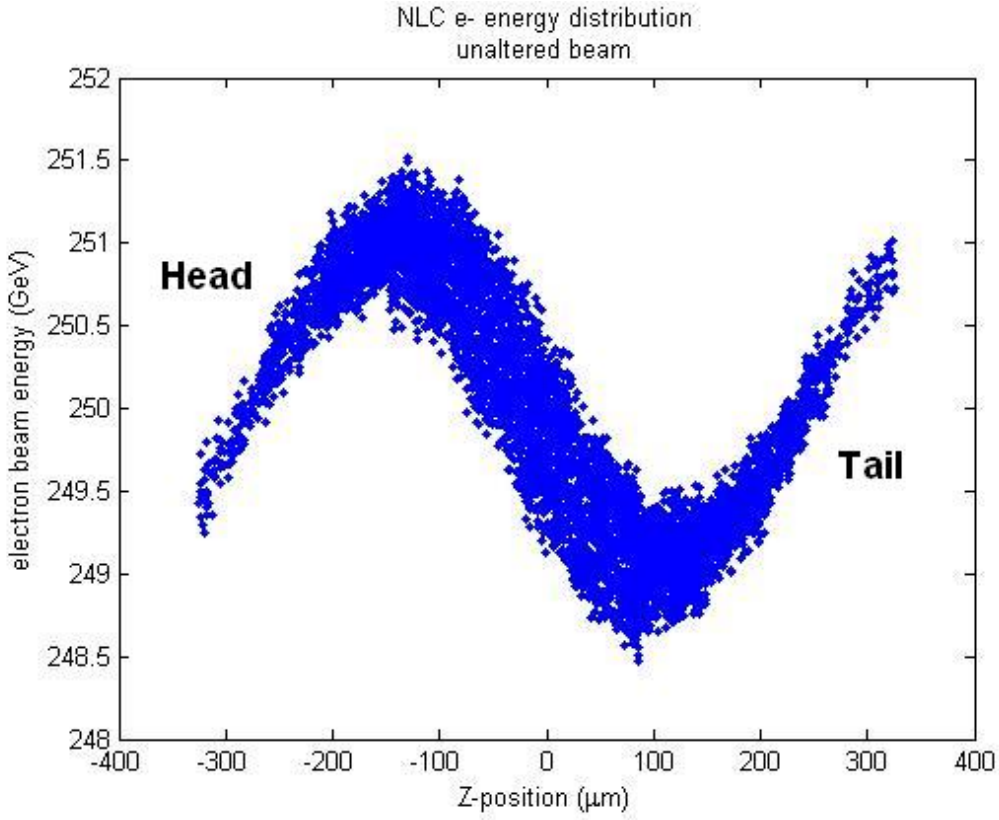

Figure 4 - Energy-z distribution of incoming beam showing head and tail. The head contains more of the higher-energy electrons, while the tail contains more of the lower-energy electrons.

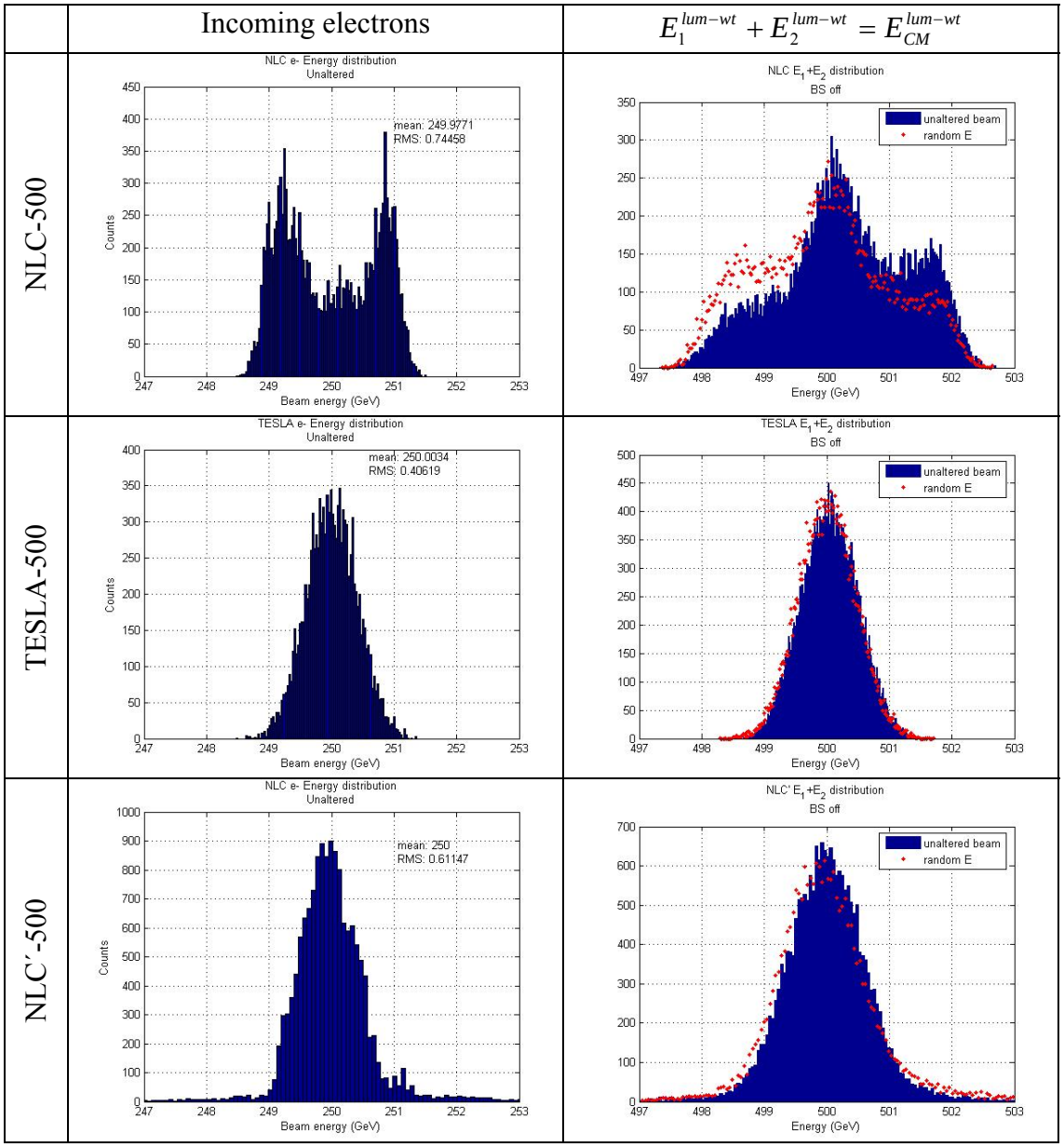

Figure 5 – Incoming beam energy (left column) and $E_1^{lum-wt} + E_2^{lum-wt} = E_{CM}^{lum-wt}$ distributions (right column) for e^+e^- collisions for three LC parameter sets (NLC, TESLA, NLC′). See section 3.1.1 for an explanation of the "unaltered beam" and "random E" distributions. The difference between these distributions reflects $E_{CM}^{bias}\Big|_{BSoff}$.

The results for $E_{CM}^{bias}\Big|_{BSoff}$ for the distributions shown in Figure 5 are +550 ppm, +95 ppm, and +8 ppm for NLC-500, TESLA-500, and NLC′-500, respectively.

3.1.2 Effects in e^-e^- collisions

This analysis was also performed for the e^-e^- mode. To run GP in e^-e^- mode, I used the same incoming distributions (*electron.ini* and *positron.ini*) and change the sign of the "charge" flag in the *acc.dat* GP input file. This flag is set to a value of -1 for e^+e^- collisions and +1 for e^-e^- collisions.

[Note: for TESLA e^-e^- collisions, I actually did not simply use a pair of *electron.ini* and *positron.ini* files. In the TESLA design, there is an undulator in the electron beam path that is used to create positrons, which causes the electron beam to have a larger energy spread than it would otherwise. In order to achieve realistic energy spread for both electron beams in an e^-e^- collision, I use for example *positron1.ini* for one beam and *positron2.ini* for the second beam.]

An example of the results for the E_{CM}^{lum-wt} is shown in Figure 6.

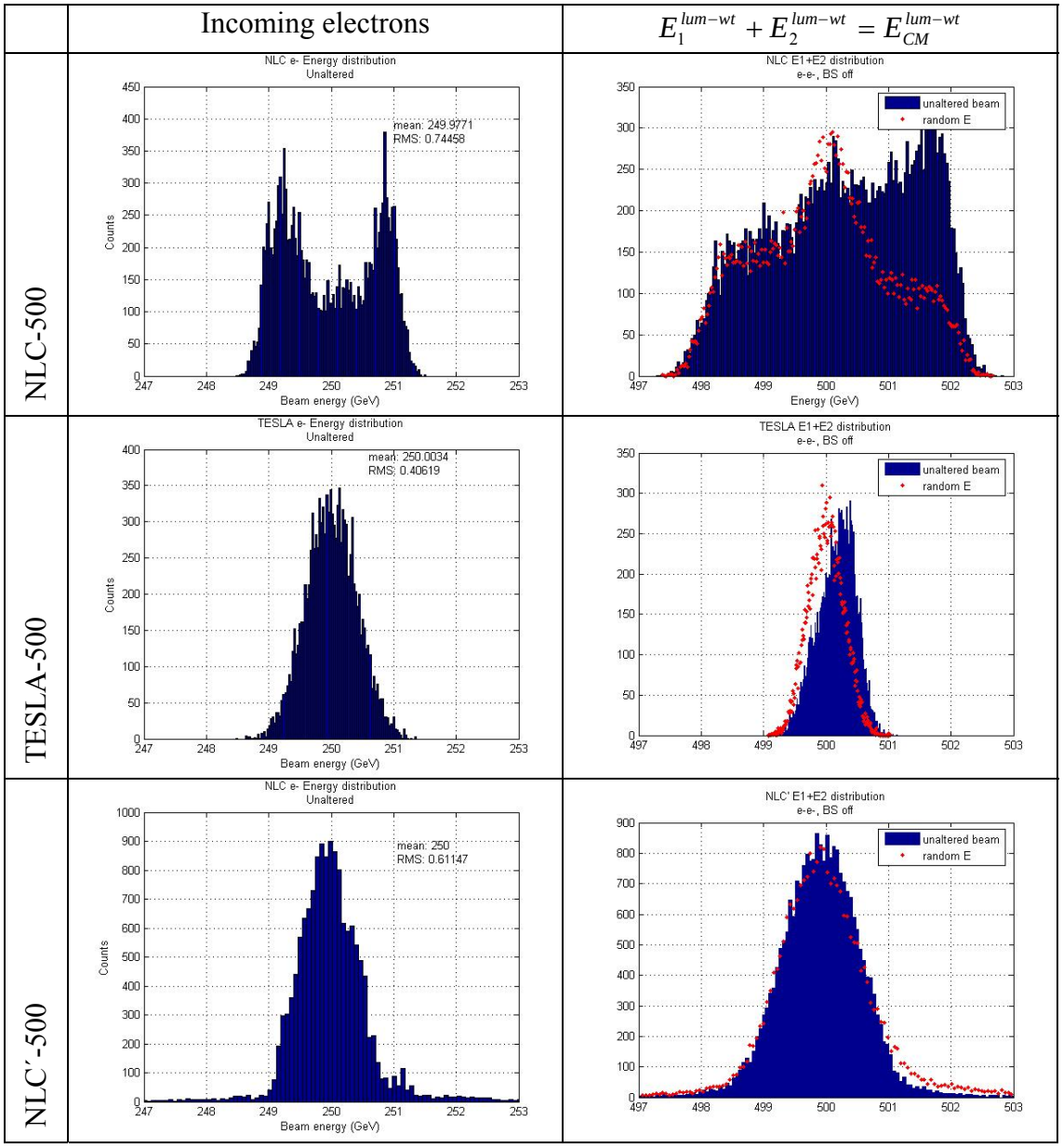

Figure 6 - Incoming beam energy (left column) and $E_1^{lum-wt} + E_2^{lum-wt} = E_{CM}^{lum-wt}$ distributions (right column) for e^-e^- collisions for three LC parameter sets (NLC, TESLA, NLC′). See section 3.1.1 for an explanation of the "unaltered beam" and "random E" distributions. The difference between these distributions reflects $E_{CM}^{bias}\Big|_{BSoff}$.

3.1.3 $E_{CM}^{bias}\Big|_{BSoff}$ for optimized collisions

The e^+e^- and e^-e^- collision studies were performed for thirteen different sets of TRC files: six for NLC-500, six for TESLA-500, and one additional set for NLC´-500. Each TRC file corresponds to a different set of (random) initial misalignments, which are then processed through beam tuning mechanisms to achieve nominal luminosity.

A summary of the calculations of $E_{CM}^{bias}\Big|_{BSoff}$ for these beams appears in Table 2. Note that the asymmetry persists in the e^-e^- collisions as well, with the values of $E_{CM}^{bias}\Big|_{BSoff}$ approximately three times larger for TESLA and approximately 1.5 times larger for NLC. There is also a much larger spread in the $E_{CM}^{bias}\Big|_{BSoff}$ results for e^-e^- collisions.

Table 2 - E_{CM}^{bias} in parts per million (ppm) for different TRC files for three LC designs, in the absence of beamsstrahlung ($E_{CM}^{bias}\Big|_{BSoff}$)

	$E_{CM}^{bias}\Big\|_{BSoff}$ *(ppm)*	
	$\mathbf{e^+e^-}$	$\mathbf{e^-e^-}$
TESLA-1	95	337
TESLA-2	71	199
TESLA-3	8	71
TESLA-4	35	235
TESLA-5	72	47
TESLA-6	36	107
Mean TESLA	*53 ± 32*	*166 ± 111*
NLC-1	545	628
NLC-2	343	1565
NLC-3	497	437
NLC-4	230	461
NLC-5	644	450
NLC-6	691	692
Mean NLC	*492 ± 177*	*706 ± 434*
NLC′	8	-159

3.1.4 $E_{CM}^{bias}\Big|_{BSoff}$ with imperfect collisions

I also investigated how various aberrations at the IP may affect $E_{CM}^{bias}\Big|_{BSoff}$. Multiple simulations were performed using GP to scan through a range of position offsets, waist offsets, and dispersion values. The results are shown in Figure 7, Figure 8, and Figure 9 for e^+e^-, and in Figure 10, Figure 11, and Figure 12 for e^-e^-. The results from a single set of TRC files are shown, but these results are illustrative of the general behavior.

The plots demonstrate that for both e^+e^- and e^-e^- collisions, all three designs are sensitive to movement away from optimal settings of offset and dispersion. Particularly in the NLC-500 and TESLA-500 designs, $E_{CM}^{bias}\Big|_{BSoff}$ rises rapidly as the offset or dispersion values move away from optimal. For NLC', there is a noticeable increase in this bias as the offset increases.

Also, the luminosity drops away quickly for all three designs as offset or dispersion moves away from nominal. This is particularly noteworthy in e^-e^- collisions, because they are more sensitive to offsets and other beam distortions due to the large anti-pinch effect (H_D in Table 1 on page 7).

It is also interesting that the maximum luminosity does not always occur at zero offset or zero dispersion. However, the maximum luminosity does occur at the same offset as the minimum value of $E_{CM}^{bias}\Big|_{BSoff}$. This is also at or about the same offset/dispersion setting as zero beam deflection.

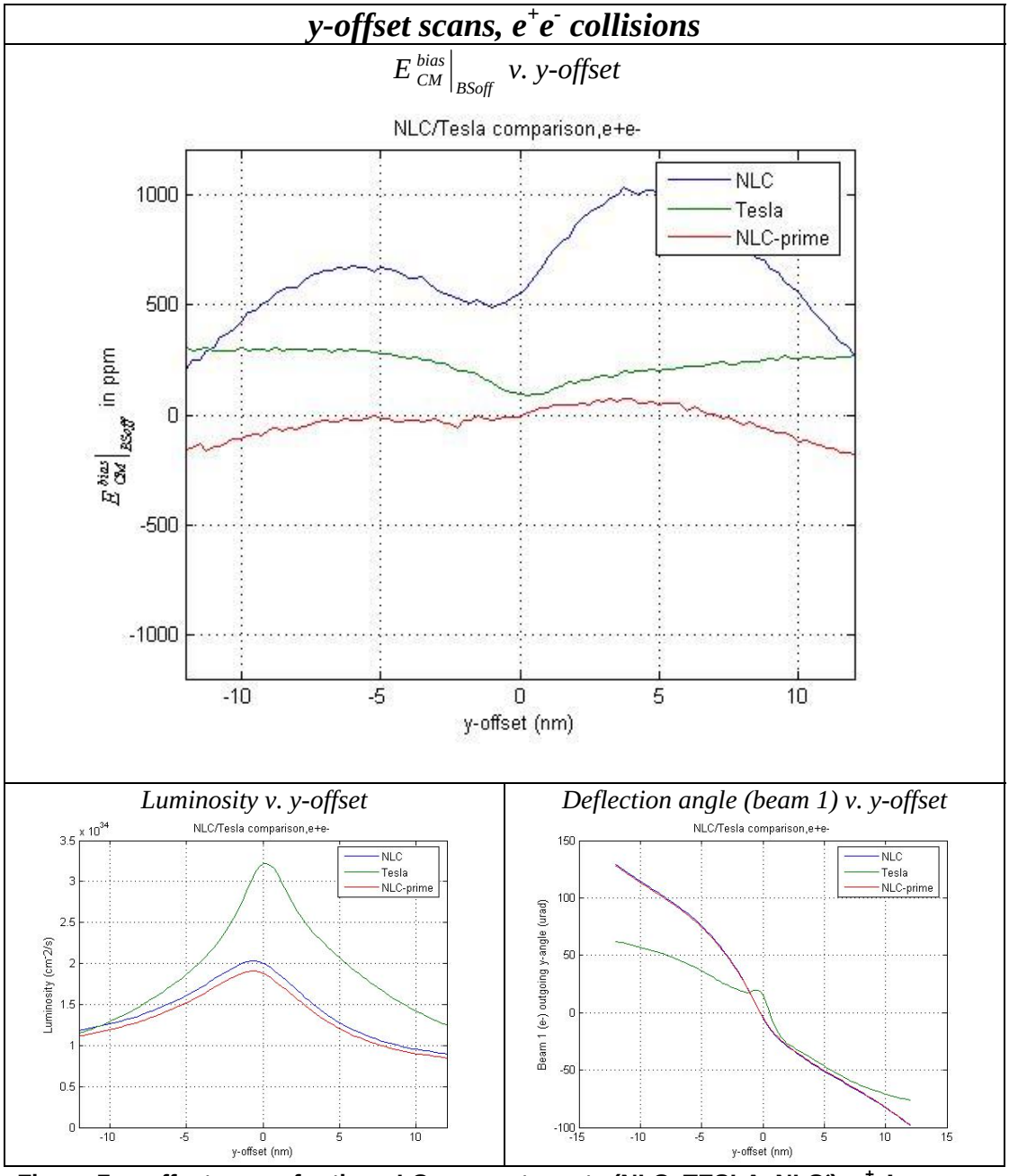

Figure 7- y-offset scans for three LC parameter sets (NLC, TESLA, NLC′), e^+e^- collisions, in the absence of beamsstrahlung. All three machines show similar behavior. Top graph shows $E_{CM}^{bias}\big|_{BSoff}$ increases as y-offset moves away from optimal. Lower-left graph shows luminosity decreases away from optimal y-offset. Lower-right graph shows the deflection angle increases as y-offset moves further from optimal.

y-dispersion scans, e^+e^- collisions

$E_{CM}^{bias}\Big|_{BSoff}$ *v. y-dispersion*

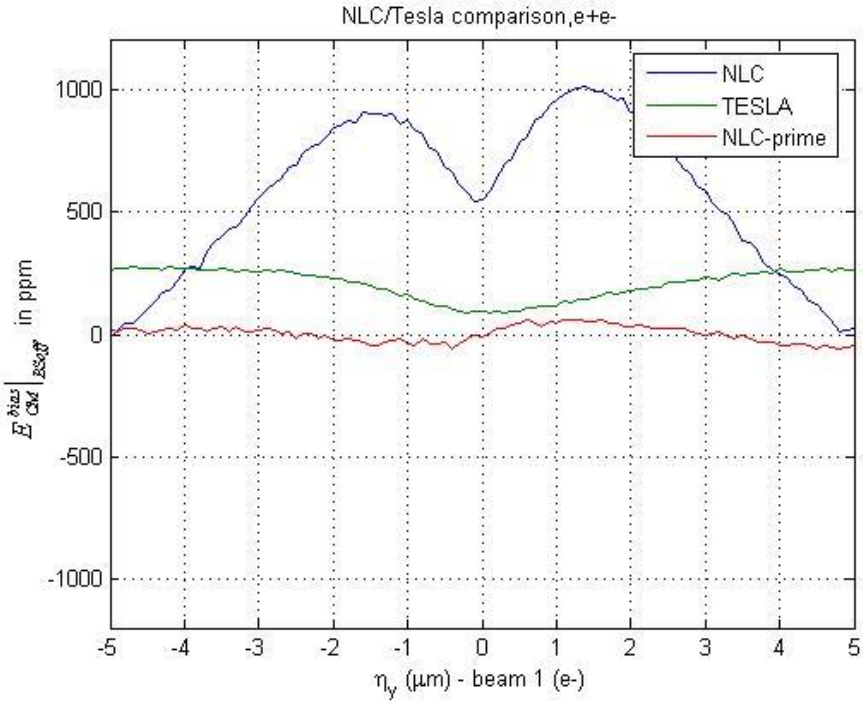

Luminosity v. y-dispersion

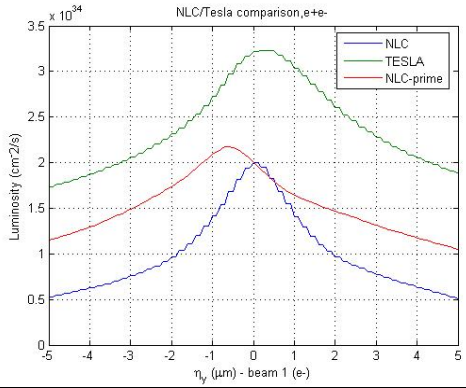

Deflection angle (beam 1) v. y-dispersion

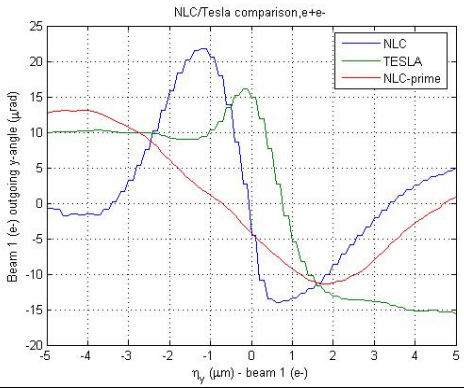

Figure 8 - y-dispersion scans for three LC parameter sets (NLC, TESLA, NLC'), e^+e^- collisions, in the absence of beamsstrahlung. Top graph shows $E_{CM}^{bias}\Big|_{BSoff}$ increases away as y-dispsersion moves away from optimal. Lower-left graph shows all three machines lose luminosity away from optimal y-dispersion. Lower-right graph shows the deflection angle is approximately zero at maximum luminosity, but increases as the y-dispersion moves from this optimal setting.

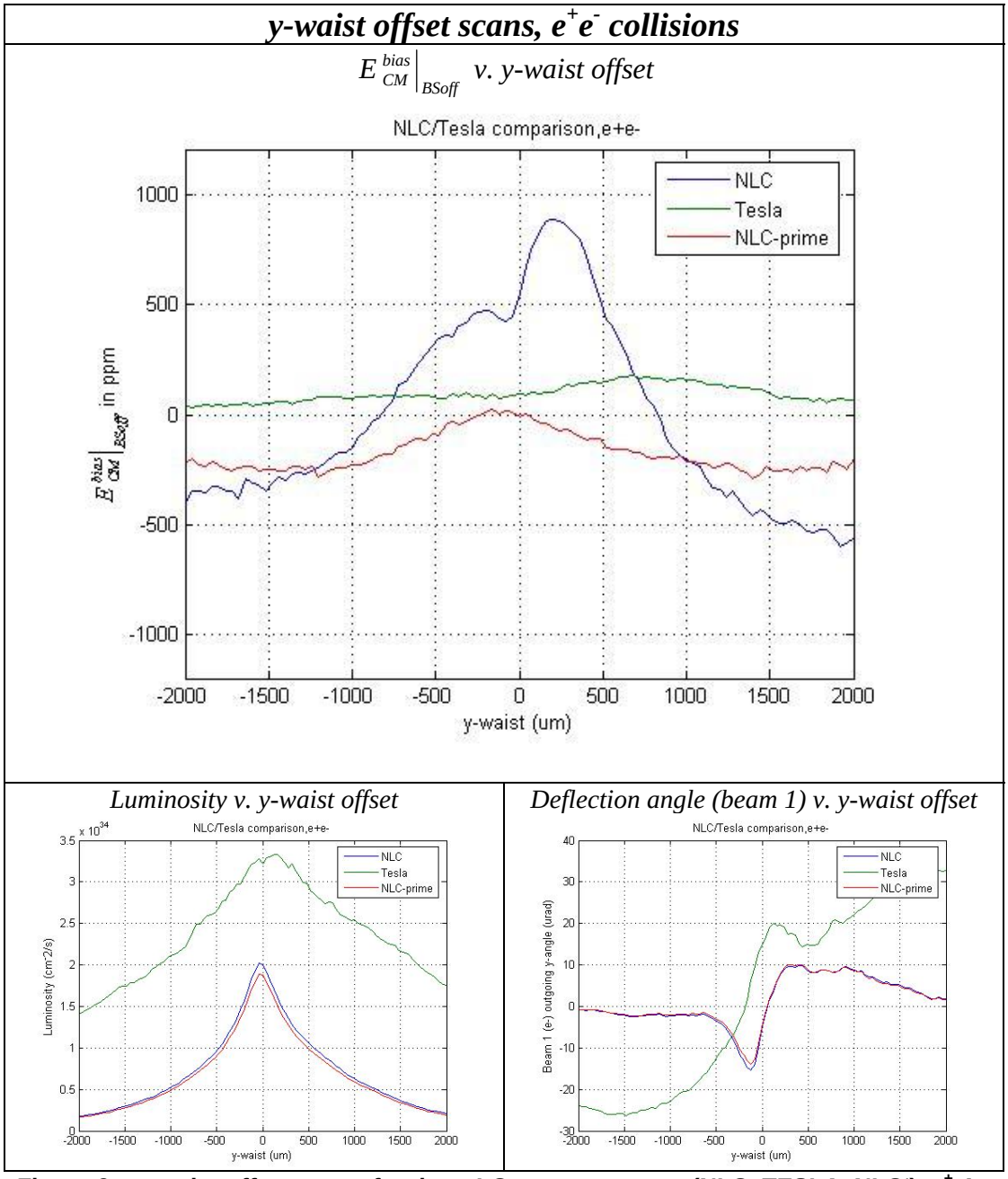

Figure 9 – y-waist-offset scans for three LC parameter sets (NLC, TESLA, NLC′), e^+e^- collisions, in the absence of beamsstrahlung. Top graph shows the magnitude of $E_{CM}^{bias}\big|_{BSoff}$ increases as y-waist is offset from optimal. Lower-left graph shows all three machines lose luminosity away from optimal y-waist offset. Lower-right graph shows the deflection angle increases the further the y-waist offset moves from optimal.

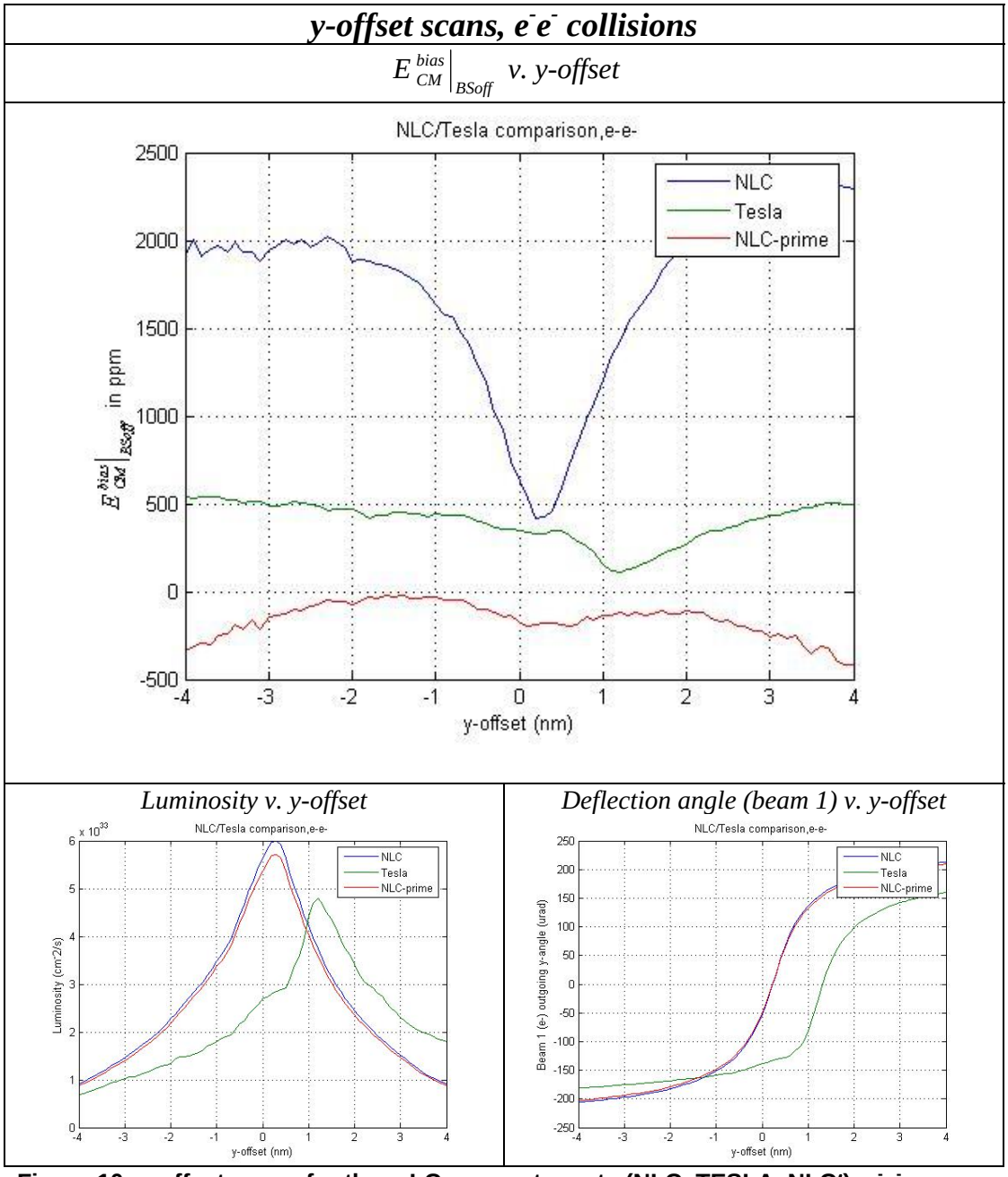

Figure 10- y-offset scans for three LC parameter sets (NLC, TESLA, NLC′), e^-e^- collisions, in the absence of beamsstrahlung. All three machines show similar behavior. Top graph shows $E_{CM}^{bias}\big|_{BSoff}$ increases as y-offset moves away from optimal. Lower-left graph shows luminosity decreases away from optimal y-offset. Lower-right graph shows the deflection angle is approximately zero at maximum luminosity, but increases as y-offset moves away from this optimal setting.

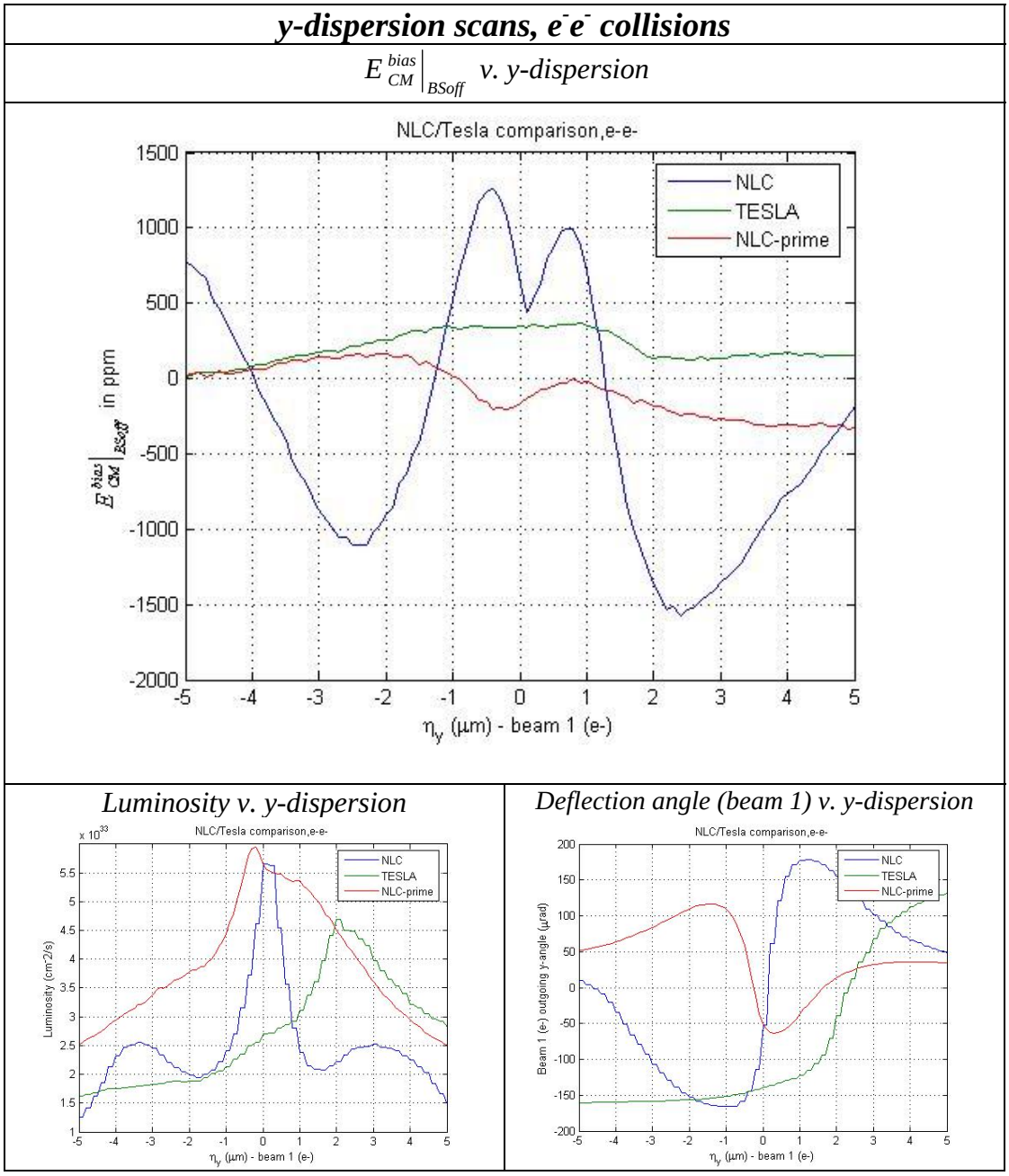

Figure 11 - y-dispersion scans for three LC parameter sets (NLC, TESLA, NLC′), e^-e^- collisions, in the absence of beamsstrahlung. Top graph shows $E_{CM}^{bias}\big|_{BSoff}$ increases away as y-dispsersion moves away from optimal for both NLC designs, but appears to hold steady for TESLA. Lower-left graph shows all three machines lose luminosity away from optimal y-dispersion. Lower-right graph shows the deflection angle is approximately zero at maximum luminosity, but increases the further the y-dispersion moves from this optimal setting.

y-waist-offset scans, e^-e^- collisions
$E_{CM}^{bias}\Big\|_{BSoff}$ *v. y-waist offset*
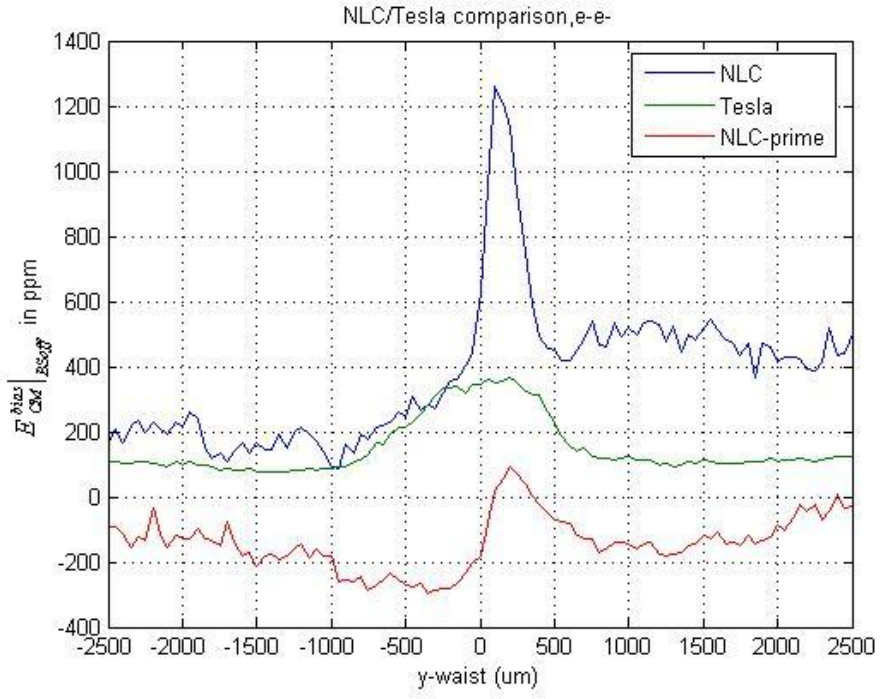
Luminosity v. y-waist offset 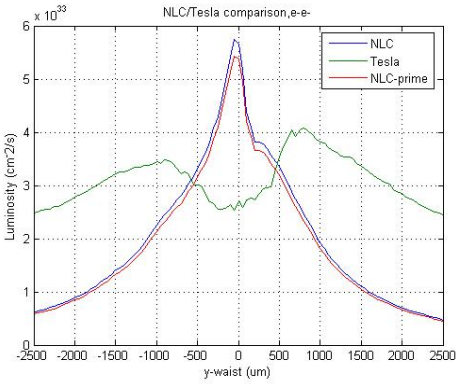 *Deflection angle (beam 1) v. y-waist offset* 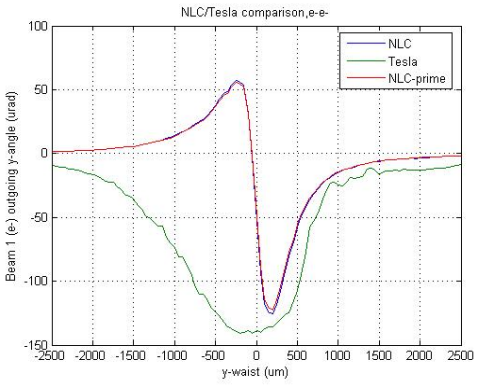

Figure 12 - y-waist-offset scans for three LC parameter sets (NLC, TESLA, NLC′), e^-e^- collisions, in the absence of beamsstrahlung. Top graph shows $E_{CM}^{bias}\Big|_{BSoff}$ decreases as y-waist is offset from optimal for all three machines. However, for NLC machines, this is accompanied by a sharp drop in luminosity (lower left graph) and the deflection angle increases the further the y-waist offset moves from optimal (lower-right graph). For TESLA, the peak luminosity occurs at a significant waist-offset (lower-left graph) which corresponds to small (nearly zero) deflection angle (lower-right).

Table 3 below summarizes $E_{CM}^{bias}\Big|_{BSoff}$ results for e^+e^- interactions, for each machine design, considering the same thirteen TRC files as before. Note that the values for $E_{CM}^{bias}\Big|_{BSoff}$ quoted so far are due to only one effect (energy spread/kink instability) and use only one analysis technique (energy spectrometers and Bhabha acolinearity).

Table 3 – Summary of E_{CM}^{bias} results for three LC parameter sets, e^+e^- collisions, in the absence of beamsstrahlung

LC Machine Design	$\left\langle E_{CM}^{bias}\Big\|_{BSoff}\right\rangle$ $\Delta y=0$, $\eta_y=0$	$\sigma\left(E_{CM}^{bias}\Big\|_{BSoff}\right)$ $\Delta y=0$, $\eta_y=0$	max $\left(E_{CM}^{bias}\Big\|_{BSoff}\right)$ vary Δy, η_y
NLC-500	+490 ppm	180 ppm	+1000 ppm
TESLA-500	+50 ppm	30 ppm	+250 ppm
NLC′-500	0 ppm	10 ppm	+50 ppm

3.2 Biases in E_{CM}^{lum-wt} in the presence of Beamsstrahlung, $E_{CM}^{bias}\Big|_{BSon}$

In the previous section, I used a GP simulation with the flags for beamsstrahlung and initial state radiation (ISR) turned off. It was found that there is a bias in $\left\langle E_{CM}^{lum-wt}\right\rangle$ on the order of 500 ppm (50 ppm) for NLC-500 (TESLA-500), where $\left\langle E_{CM}^{lum-wt}\right\rangle$ and the bias are determined by equation (1). I now study the effect of beamsstrahlung on E_{CM}^{bias} by turning on the beamsstrahlung flag in GP.

To determine the value of $E_{CM}^{bias}\Big|_{BSon}$ I again analyzed the *lumi.ee.out* files generated by GP simulations of beam-beam interactions. I used the same thirteen sets of GP input files *electron.ini* and *positron.ini*: six different sets each for NLC and TESLA, (corresponding to different beam simulation parameters) as well as the alternate phase BNS configuration NLC file (NLC′).

For each pair of input files electron.ini and positron.ini, I generated:

i) ***unaltered*** electron.ini and positron.ini,
ii) ***gaussian E*** electron.ini and positron.ini, and
iii) ***random E*** electron.ini and positron.ini files.

For the ***gaussian*** files, the E-distribution was replaced with an uncorrelated Gaussian energy distribution of the correct rms (0.3% for NLC, 0.16% (electron) and 0.08% (positron) for TESLA, and 0.24% for NLC′). For the ***random*** files, the E-distribution was unchanged but was re-ordered randomly among the ten-to-fifteen thousand particles in the *electron.ini* and *positron.ini* files (refer to Appendix A.6). Examples of the incident beam energy distributions are shown in Figure 13, and the Energy-z correlations for the incident beams are shown in Figure 14.

	NLC-500	TESLA-500	NLC′-500
Unaltered beam	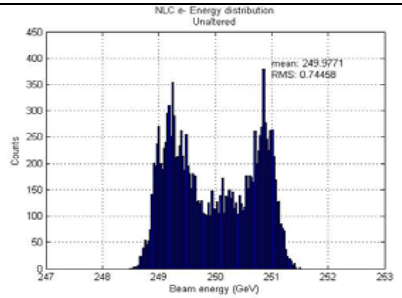	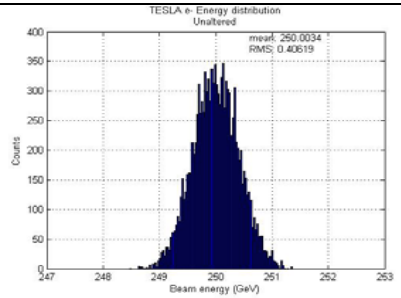	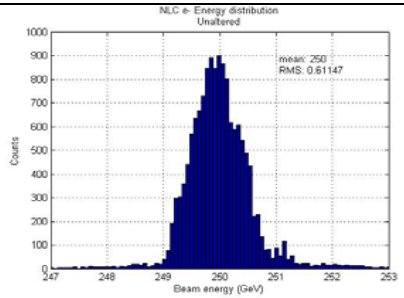
	Mean=249.97; RMS=0.745	Mean=250.00; RMS=0.406	Mean=250.00; RMS=0.61
Gaussian E	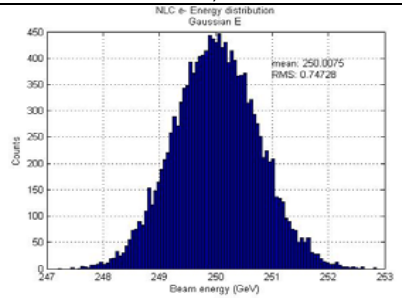	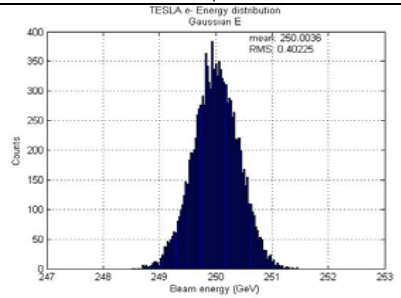	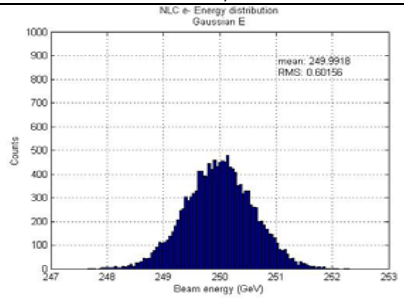
	Mean=250.01; RMS=0.747	Mean=250.00; RMS=0.401	Mean=249.99; RMS=0.60
Random E	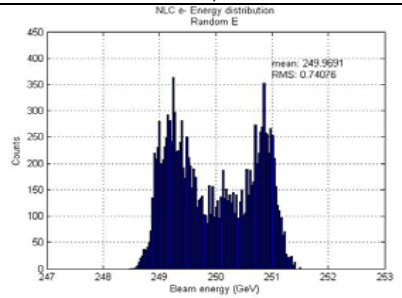	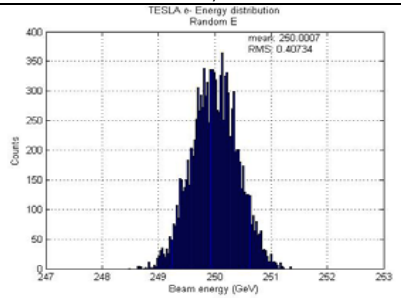	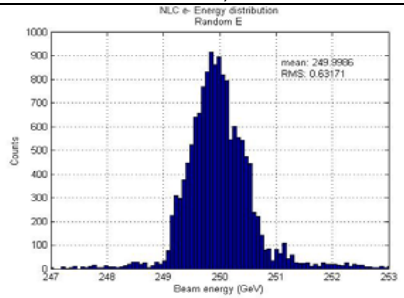
	Mean=249.97; RMS=0.741	Mean=250.00; RMS=0.402	Mean=250.00; RMS=0.63

Figure 13 – Incident beam energy distributions used in $E_{CM}^{bias}\Big|_{BSon}$ for three LC parameter sets (NLC, TESLA, NLC′) at 500 GeV. Explanation for the "unaltered beam", "Gaussian E", and "Random E" distributions are given in section 3.2.

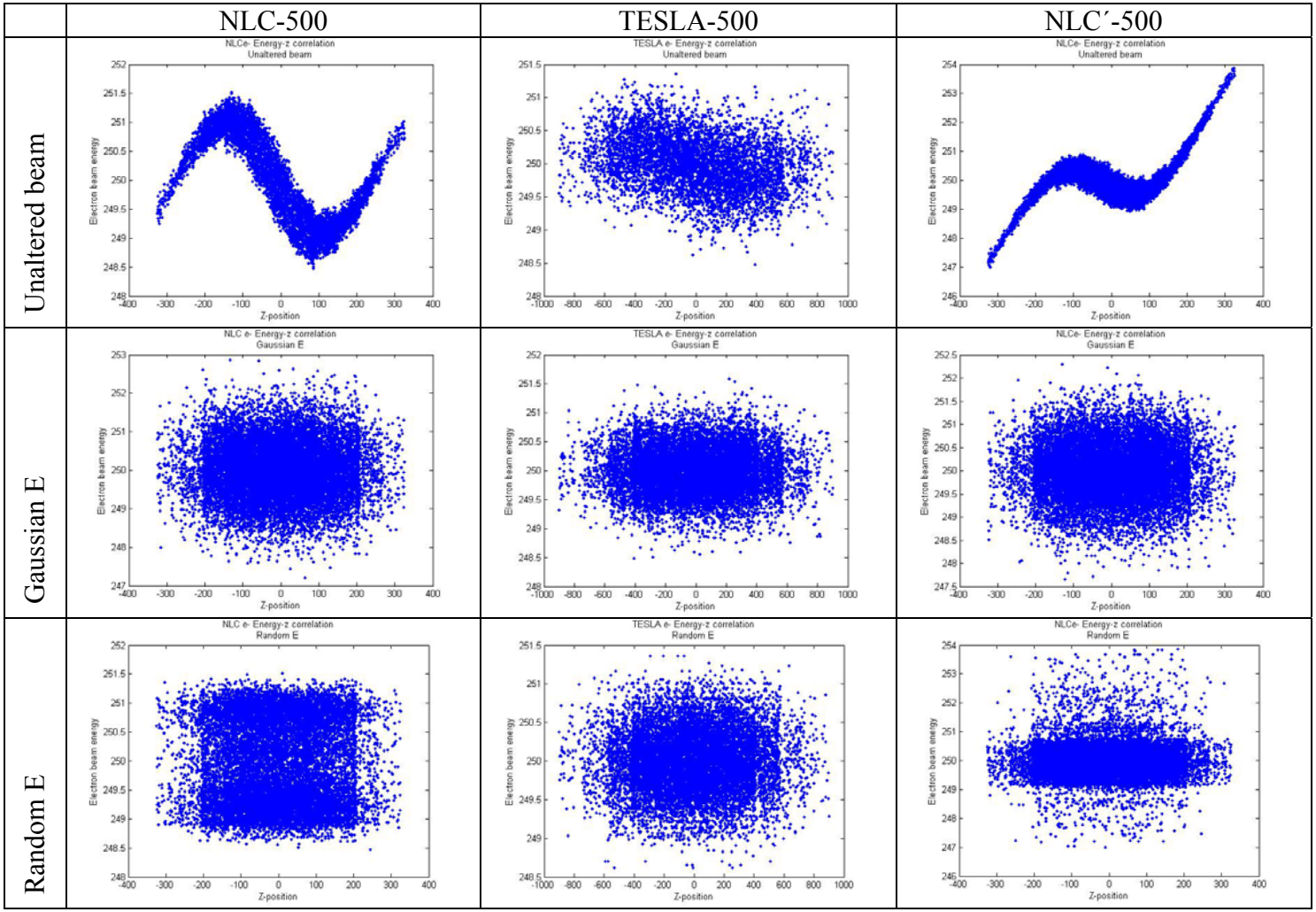

Figure 14 - Examples of Energy-z distributions for incident beams, used in $E_{CM}^{bias}\Big|_{BSon}$ for three LC parameter sets (NLC, TESLA, NLC′) at 500 GeV. Explanation for the "unaltered beam", "Gaussian E", and "Random E" distributions are given in section 3.2.

The purpose of the Gaussian-E and random-E files was to turn off the energy-z correlation of the input distributions, thereby giving a control sample with no energy bias from the kink instability. I calculated $E_{CM}^{bias}\Big|_{BSon}$ according to

$$E_{CM}^{bias}\Big|_{BSon} = \left\langle E_{CM}^{lum-wt} \right\rangle\Big|_{unaltered}^{E_{CM} > Ecutoff} - \left\langle E_{CM}^{lum-wt} \right\rangle\Big|_{randomE}^{E_{CM} > Ecutoff} \tag{2}$$

or

$$E_{CM}^{bias}\Big|_{BSon} = \left\langle E_{CM}^{lum-wt} \right\rangle\Big|_{unaltered}^{E_{CM} > Ecutoff} - \left\langle E_{CM}^{lum-wt} \right\rangle\Big|_{gaussianE}^{E_{CM} > Ecutoff} \tag{3}$$

I calculated $E_{CM}^{bias}\Big|_{BSon}$ considering interactions that had a center-of-mass energy greater than a certain cutoff. The cutoff energy was varied between 480 GeV and 495 GeV to study the stability of the results. Varying the cutoff value made only marginal difference in the results, in each case within one standard deviation of each other. The cutoff value of 495 GeV was chosen because it eliminates some of the fluctuations caused by events with large beamsstrahlung losses, while still preserving the core of the interaction spectrum (the cutoff of 495 GeV is $\geq 5\ \sigma$ from the mean for the incident energy spread for each of NLC, TESLA, and NLC', and $\geq 60\%$ of the events fall above this cutoff). Figure 15 shows the cutoff of 495 GeV for the NLC example. The main results quoted are computed using the 495 GeV cutoff.

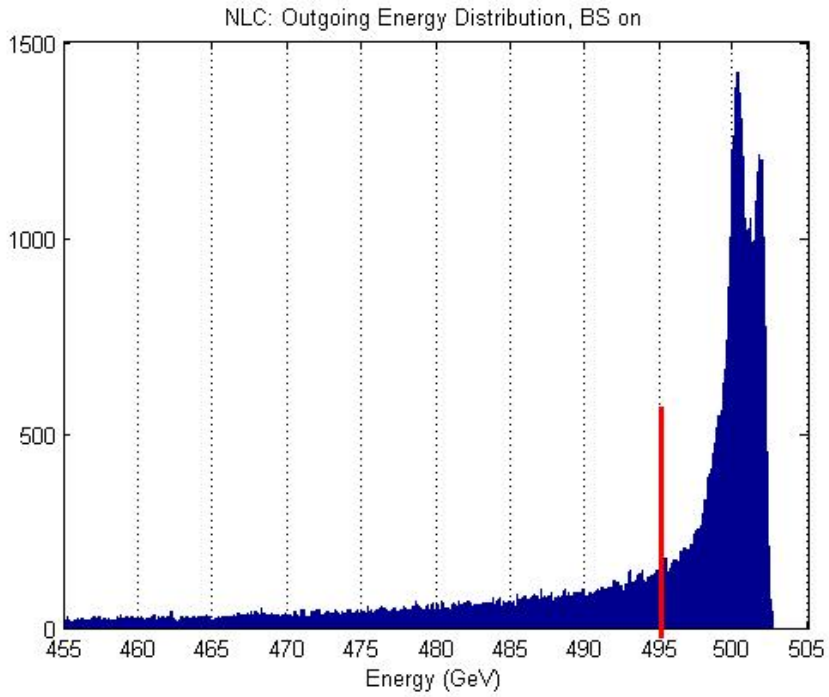

Figure 15- E_{CM}^{lum-wt} distribution in the presence of beamsstrahlung for one NLC file showing 495GeV cutoff. The cutoff is 5 σ(E) below the peak. 60 percent of all events fall above the 495 GeV cutoff.

3.2.1 $E_{CM}^{bias}\Big|_{BSon}$ for optimized collisions

For each of the thirteen sets of input files considered, a GP simulation was run with unaltered input files to calculate $\left\langle E_{CM}^{lum-wt}\right\rangle\Big|_{unaltered}^{E_{CM}>Ecutoff}$. A second simulation was run to calculate $\left\langle E_{CM}^{lum-wt}\right\rangle\Big|_{gaussianE}^{E_{CM}>Ecutoff}$, and finally a third simulation to calculate $\left\langle E_{CM}^{lum-wt}\right\rangle\Big|_{randomE}^{E_{CM}>Ecutoff}$. This was repeated five times for each set of input files, each time using a different random number seed. The results of each run were tabulated and the

mean was taken. The results for these values and for the calculated value of $E_{CM}^{bias}\big|_{BSon}$ are shown in Table 4 and Table 5. The standard deviation in the value of $E_{CM}^{bias}\big|_{BSon}$ for any given set of data files was found to be between 20 and 60 ppm, which reflects the statistical uncertainty in the results. The error bars quoted in the table refer to the standard deviation between the six different input files for each of NLC and TESLA.

The plots in Figure 16 summarize these results graphically for $E_{CM}^{bias}\big|_{BSon}$ and $E_{CM}^{bias}\big|_{BSoff}$. Prior to doing the study with beamsstrahlung considered, it was expected that when the effects of beamsstrahlung were factored in, the results for $E_{CM}^{bias}\big|_{BSon}$ would be very similar to the results for $E_{CM}^{bias}\big|_{BSoff}$ seen earlier. However, from the results it is clear that the effect is in fact exacerbated, by roughly a factor of three for TESLA and a factor of two for NLC. For NLC′, the optimal BNS configuration, there was only one TRC file set to work with, but the results from that set hint that BS increases the bias as well.

Table 4- E_{CM}^{bias} **in parts per million (ppm) in the presence of beamsstrahlung. Results shown here utilize a Gaussian input energy distribution as described in section 3.2, and require** E_{CM} **> 495 GeV**

	$E_{CM}^{bias}\big\vert_{BSoff}$	$\left\langle E_{CM}^{lum-wt}\right\rangle\Big\vert_{unaltered}^{E_{CM}>Ecutoff}$	$\left\langle E_{CM}^{lum-wt}\right\rangle\Big\vert_{gaussianE}^{E_{CM}>Ecutoff}$	$E_{CM}^{bias}\big\vert_{BSon}$
TESLA-1	95	-1371	-1567	**197**
TESLA-2	71	-1365	-1582	**217**
TESLA-3	8	-1474	-1598	**123**
TESLA-4	35	-1473	-1618	**146**
TESLA-5	72	-1426	-1645	**219**
TESLA-6	36	-1493	-1644	**150**
Mean TESLA	*53 ± 32*	*-1434 ± 55*	*-1609 ± 32*	***175** ± **41***
NLC-1	545	-228	-1269	**982**
NLC-2	343	-413	-1301	**921**
NLC-3	497	-300	-1266	**944**
NLC-4	230	-570	-1309	**770**
NLC-5	644	-192	-1249	**1026**
NLC-6	691	-126	-1236	**1308**
Mean NLC	*492 ± 177*	*-305 ± 163*	*-1272 ± 29*	***967** ± **136***
NLC′	8	-1278	-1205	**-73**

Table 5 - E_{CM}^{bias} **in parts per million (ppm) in the presence of beamsstrahlung. Results shown here utilize a randomly re-ordered input energy distribution to remove energy-Z correlations as described in section 3.2, and require** E_{CM} **> 495 GeV**

	$E_{CM}^{bias}\big\vert_{BSoff}$	$\left\langle E_{CM}^{lum-wt}\right\rangle\Big\vert_{unaltered}^{E_{CM}>Ecutoff}$	$\left\langle E_{CM}^{lum-wt}\right\rangle\Big\vert_{randomE}^{E_{CM}>Ecutoff}$	$E_{CM}^{bias}\big\vert_{BSon}$
TESLA-1	95	-1371	-1542	**171**
TESLA-2	71	-1365	-1545	**180**
TESLA-3	8	-1474	-1572	**97**
TESLA-4	35	-1473	-1587	**115**
TESLA-5	72	-1426	-1593	**167**
TESLA-6	36	-1493	-1643	**149**
Mean TESLA	*53 ± 32*	*-1434 ± 55*	*-1580 ± 37*	***147** ± **33***
NLC-1	545	-228	-1260	**1032**
NLC-2	343	-413	-1284	**871**
NLC-3	497	-300	-1271	**971**
NLC-4	230	-570	-1266	**697**
NLC-5	644	-192	-1295	**1104**
NLC-6	691	-126	-1194	**1069**
Mean NLC	*492 ± 177*	*-305 ± 163*	*-1262 ± 36*	***957** ± **152***
NLC′	8	-1278 ± 28	-1246 ± 13	**-32** ± **22**

	E_{CM}^{bias} in the presence of Beamsstrahlung
Gaussian E	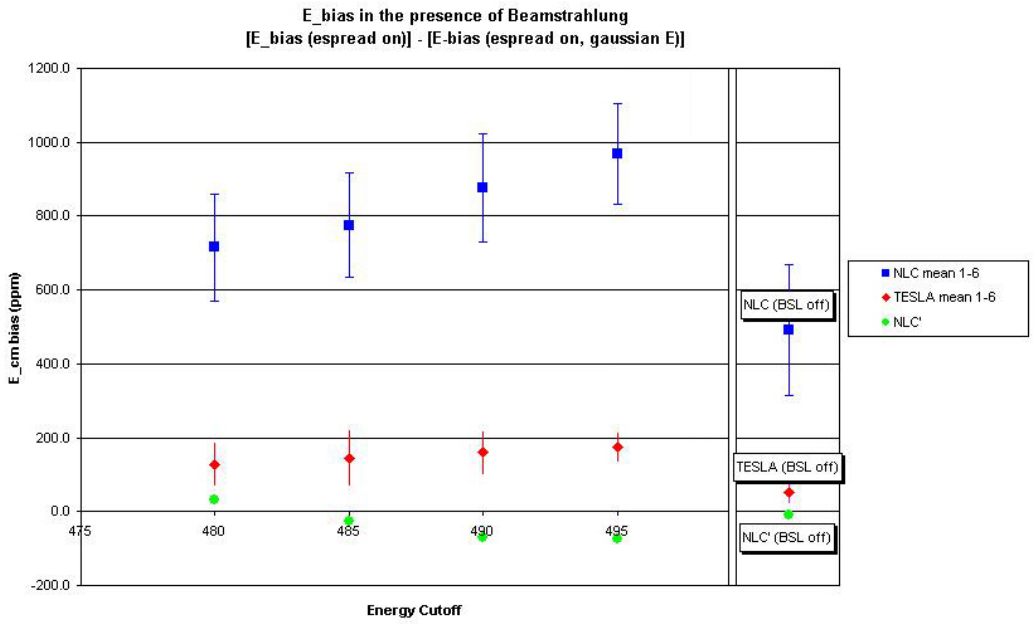
Random E	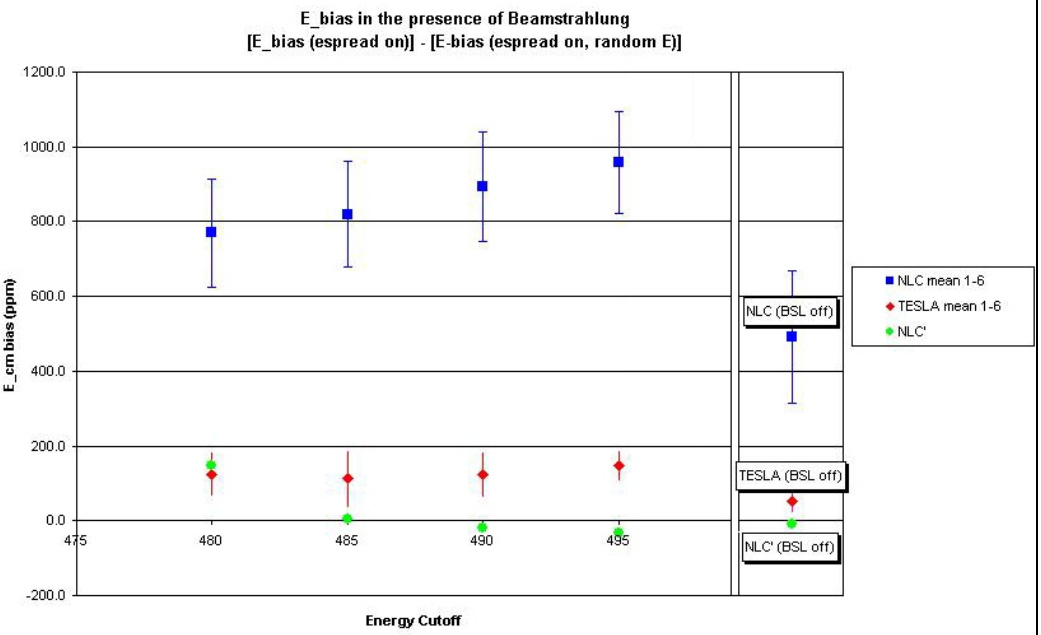

Figure 16 - Results for $E_{CM}^{bias}\Big|_{BSon}$ calculated for $E_{CM} > E_{Cutoff}$ (plotted on the main axes) and $E_{CM}^{bias}\Big|_{BSoff}$ (plotted on the right). Similar results are seen for both reference input energy distributions—Gaussian and random. Explanations for the Gaussian-E and Random-E distributions is given in section 3.2.

3.2.2 $E_{CM}^{bias}\big|_{BSon}$ for imperfect collisions

Earlier I examined the dependence of $E_{CM}^{bias}\big|_{BSoff}$ with varying vertical beam offsets and vertical dispersion (see Figure 7, Figure 8, and Figure 9). In this part of the study I examine these dependencies again in the presence of beamsstrahlung.

The results are summarized graphically in the following figures. Figure 17 and Figure 18 show the y-offset and y-dispersion scans compared for all three machine designs. Figure 19, Figure 20, and Figure 21 show comparisons of $E_{CM}^{bias}\big|_{BSoff}$ with that for $E_{CM}^{bias}\big|_{BSon}$ with both Gaussian-E and Random-E for the three machine designs, NLC, TESLA, and NLC'. Table 6 summarizes the values found for e^+e^- interactions in the presence of beammstrahlung (refer back to Table 3 on page 28 for the analogous table with beamsstrahlung effects switched off). For all machine designs, E_{CM}^{bias} can be significantly larger for imperfect collisions, and this is true when beamsstrahlung is present or absent.

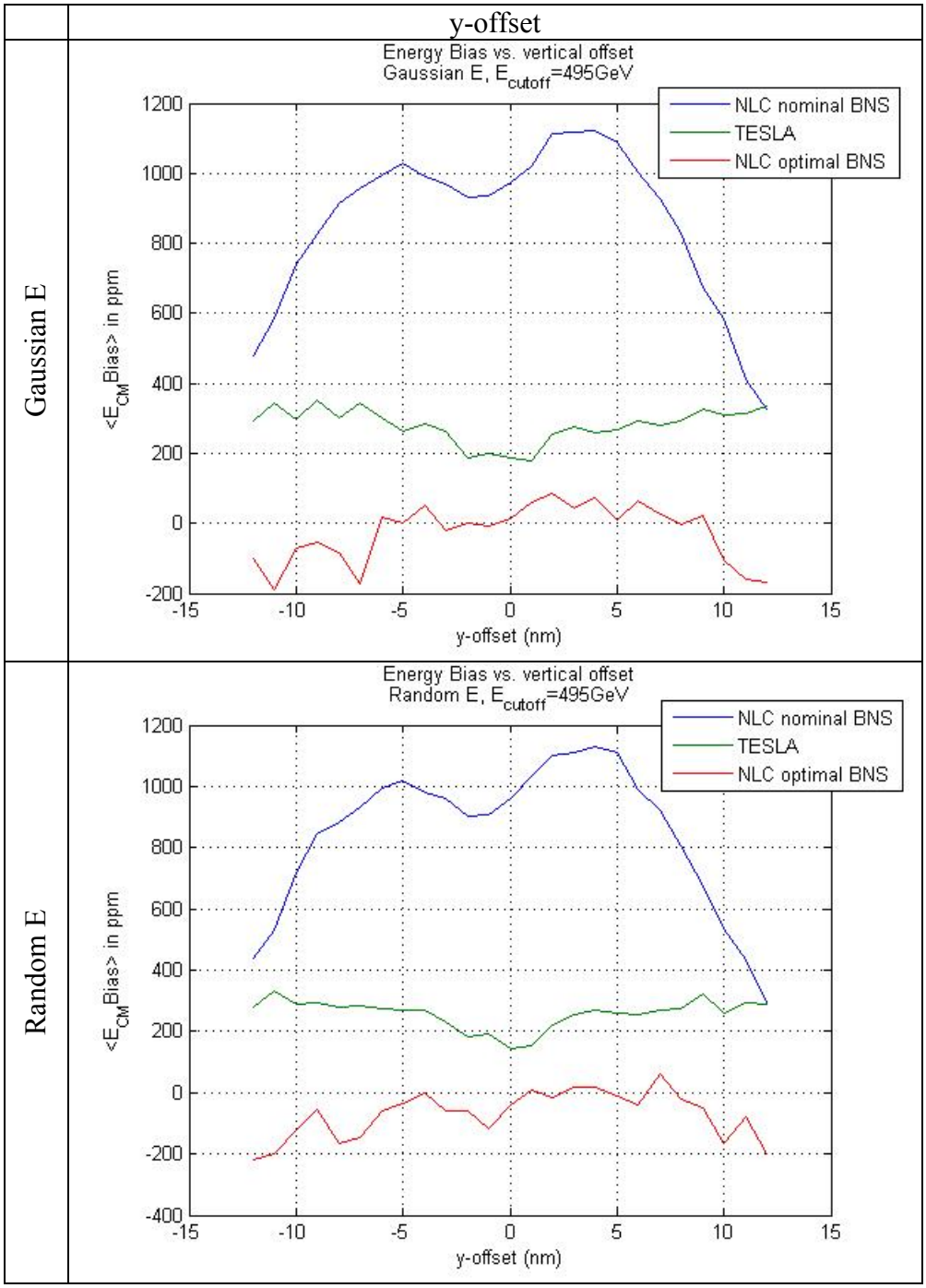

Figure 17 - $E_{CM}^{bias}\Big|_{BSon}$ **vs. y-offset, results for e+e- collisions for three LC parameter sets (NLC, TESLA, NLC′) at 500 GeV. "Gaussian E" and "Random E" reference distributions are used as part of the calculation of** $E_{CM}^{bias}\Big|_{BSon}$ **. Further explanation is given in section 3.2.**

	y-dispersion
Gaussian E	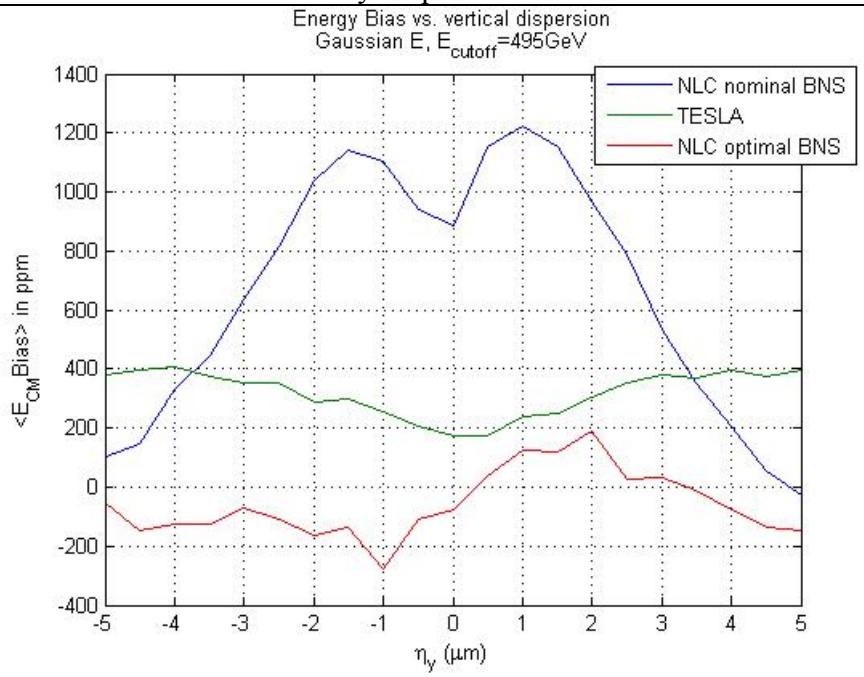
Random E	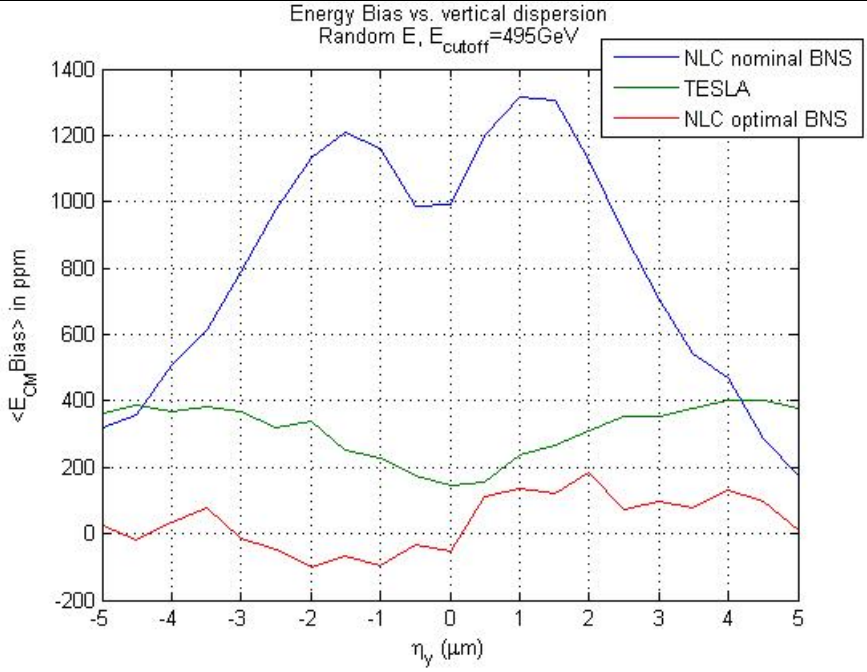

Figure 18 - $E_{CM}^{bias}\Big|_{BSon}$ **vs. y-dispersion results for e+e- collisions for three LC parameter sets (NLC, TESLA, NLC') at 500 GeV. "Gaussian E" and "Random E" reference distributions are used as part of the calculation of** $E_{CM}^{bias}\Big|_{BSon}$ **. Further explanation is given in section 3.2.**

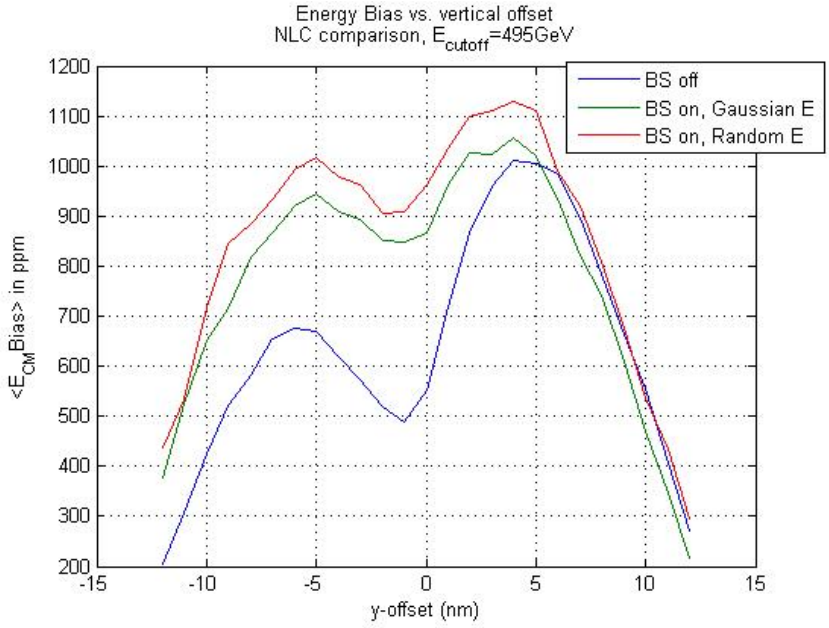

Figure 19 - $E_{CM}^{bias}\Big|_{BSon}$ **vs. y-offset results for NLC machine design.** E_{CM}^{bias} **increases when beamsstrahlung is considered, and** E_{CM}^{bias} **is bias is sensitive to imperfect collisions whether beamsstrahlung is present or absent.**

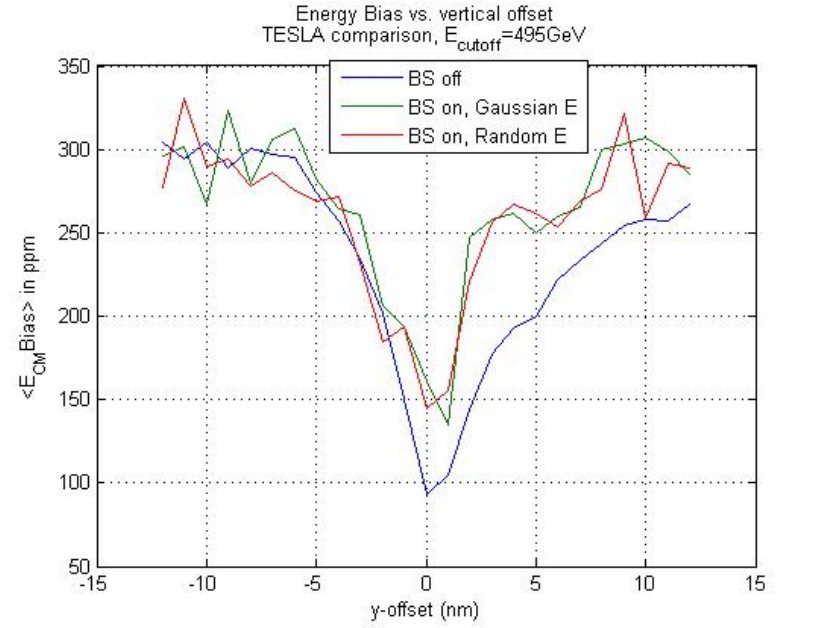

Figure 20 - $E_{CM}^{bias}\Big|_{BSon}$ **vs. y-offset results for TESLA machine design.** E_{CM}^{bias} **increases when beamsstrahlung is considered, and** E_{CM}^{bias} **is bias is sensitive to imperfect collisions whether beamsstrahlung is present or absent.**

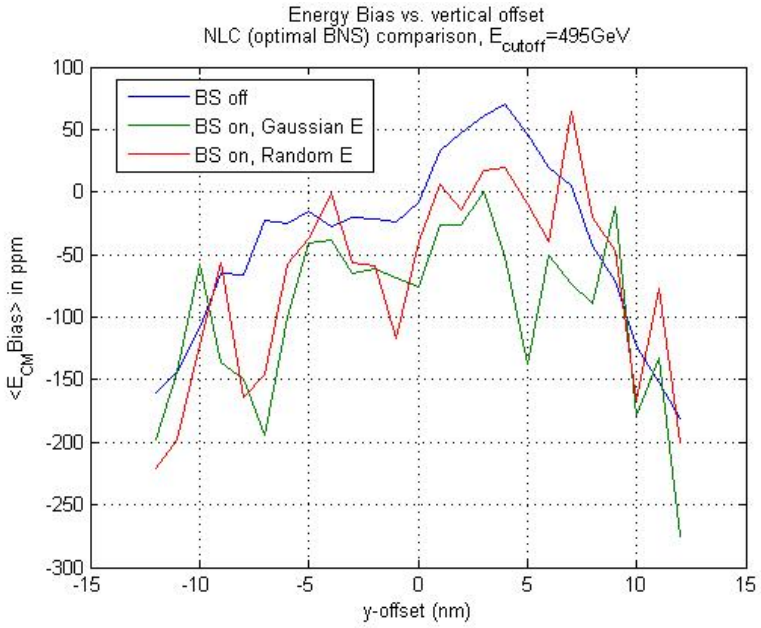

Figure 21 - $E_{CM}^{bias}\Big|_{BSon}$ **vs. y-offset results for NLC′ machine design,** E_{CM}^{bias} **increases when beamsstrahlung is considered, and** E_{CM}^{bias} **is bias is sensitive to imperfect collisions whether beamsstrahlung is present or absent.**

Table 6 – Summary of E_{CM}^{bias} **results for three LC parameter sets (NLC, TESLA, and NLC′), e^+e^- collisions, in the presence of beamsstrahlung**

LC Machine Design	$\langle E_{CM}^{bias} \rangle$ $\Delta y=0, \eta_y=0$	$\sigma(E_{CM}^{bias})$ $\Delta y=0, \eta_y=0$	max (E_{CM}^{bias}) vary $\Delta y, \eta_y$
NLC-500	+960 ppm	150 ppm	+1300 ppm
TESLA-500	+150 ppm	30 ppm	+400 ppm
NLC′-500	-30 ppm	20 ppm	+150 ppm

3.3 Bhabha acolinearity study

One method for reconstructing the luminosity spectrum is to utilize energy spectrometers and Bhabha acolinearity. The difference in the energies in the incident particles leads to an angle $\Delta\theta$ between the outgoing beams. Bhabha scattering is illustrated in Figure 22, where the acolinearity angle $\Delta\theta$ is defined.

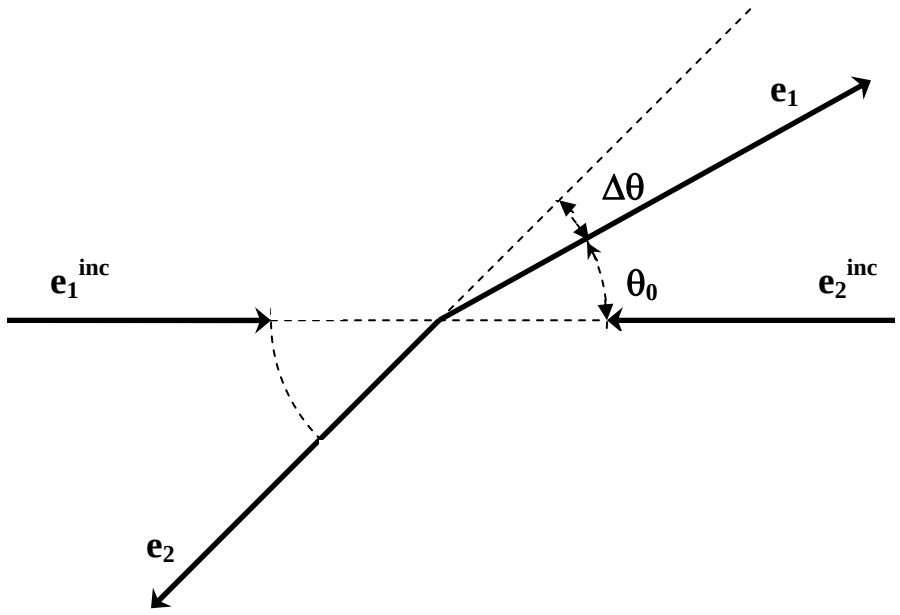

Figure 22 - Bhabha scattering after radiation loss by the incoming particle e_2^{inc} due either to ISR or beamsstrahlung. The acolinearity angle $\Delta\Theta$ arises from the energy difference in the incoming particles e_1^{inc} and e_2^{inc}.

It is assumed that only one beam radiates and that the colliding beams are collinear. In the scattering example in Figure 22, particle e_2 has radiated and lost energy. Conservation of momentum in this interaction yields two equations:

$$p_2 \cdot \sin(\Theta_0 + \Delta\Theta) = p_1 \cdot \sin\Theta_0 \quad (4)$$

$$\Delta p = p_1^{inc} - p_2^{inc} = p_1 \cdot \cos\Theta_0 - p_2 \cdot \cos(\Theta_0 + \Delta\Theta) \quad (5)$$

For sufficiently small $\Delta\Theta$, these equations reduce to:

$$p_2 \cdot [\sin\Theta_0 + \Delta\Theta \cdot \cos\Theta_0] = p_1 \cdot \sin\Theta_0 \quad (6)$$

$$\Delta p = p_1 \cdot \cos\Theta_0 - p_2 \cdot [\cos\Theta_0 - \Delta\Theta \cdot \sin\Theta_0] \quad (7)$$

From this Δp can be found:

$$\Delta p = \frac{\Delta\Theta \cdot p_1}{\sin\Theta_0} \quad (8)$$

The observed center-of-mass energy (luminosity spectrum), $\sqrt{s'}$, and expected center-of-mass energy in the absence of ISR or beamsstrahlung, $\sqrt{s}$ = 500 GeV (will be measured by the energy spectrometers), are given by:

$$\sqrt{s'} = E_1^{lum-wt} + E_2^{lum-wt} = p_1 + p_2$$

$$\sqrt{s} = \sqrt{s'} + \Delta p = 2 \cdot p_{beam}$$

With the assumption that e_1^{inc} has not radiated, we have $p_1 = p_{beam}$. The observed luminosity spectrum can then be determined from beam spectrometer energy measurements and forward tracking measurements:

$$\frac{\sqrt{s'}}{\sqrt{s}} = 1 - \frac{\Delta p}{2 \cdot p_{\text{beam}}} = 1 - \frac{\Delta\Theta}{2 \cdot \sin\Theta}$$

It is noted that $E_{CM}^{bias}\Big|_{BSon}$ would be observable if the Bhabha energies, E_1 and E_2, could be accurately measured. In this study, I simulated the (E_1+E_2) distribution using the energies of the particles that create luminosity, as listed in the GP output file *lumi.ee.out*. In the left half of Figure 23 are graphs of the quantity (E_1+E_2) for three different sets of beam parameters. There are very clear differences in the distributions. However, the quantity (E_1+E_2) is not observable because the detector energy resolution and systematics are not expected to be good enough[8,9]. The primary calorimeter candidates being considered target an energy resolution of approximately $10\%/\sqrt{E(GeV)}$[11,12]. At a center-of-mass energy of 500GeV, this corresponds to an energy resolution of 4500ppm – clearly not precise enough to resolve the features seen in Figure 23.

Bhabha acolinearity measurements are expected to accurately measure the acolinearity angle. This would yield the energy distribution (E_1-E_2). In the right half of Figure 23, we plot the GP simulation results for the distribution (E_1-E_2), again using the energies of the particles that create luminosity from *lumi.ee.out*. Examination of the distributions in Figure 23 indicates no appreciable differences between an E-Z correlated beam and a randomized beam. Thus the Bhabha acolinearity cannot be used observe or resolve the energy bias studied here. In order to understand the luminosity spectrum to the 50-200 ppm level, one alternative may

be to rely on either improved calorimeter systematics or analysis of physics results for other channels, such as $e^+e^- \rightarrow Z\gamma \rightarrow f\bar{f}\gamma$; $e^+e^- \rightarrow Z^+Z^-$; $e^+e^- \rightarrow W^+W^-$. Alternatively, it may be possible to rely on simulations as presented in this study. But these require very accurate measurements of the colliding beam parameters and the uncertainties may be larger than the targeted precision of 50-200 ppm.

	E_1+E_2, compare unaltered with "Random E"	E_1-E_2, compare unaltered with "Random E"
NLC	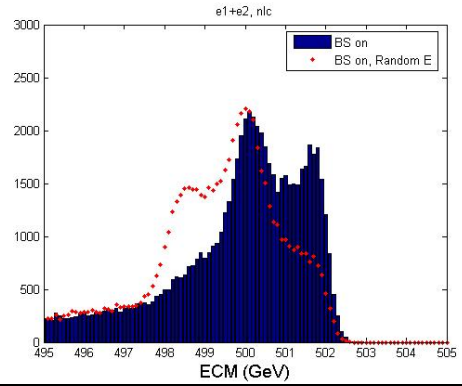	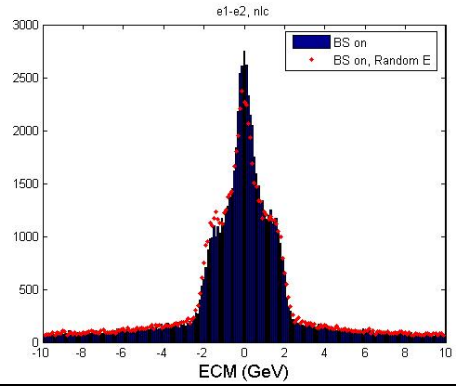
TESLA	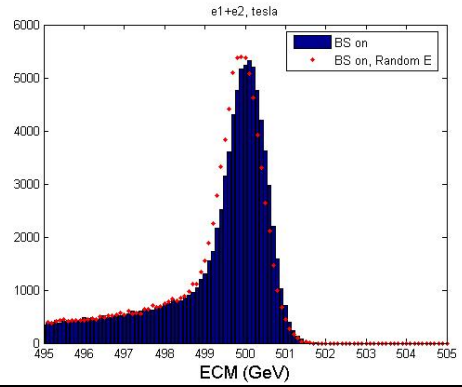	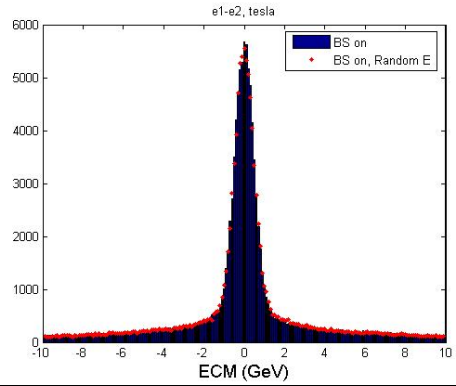
NLC'	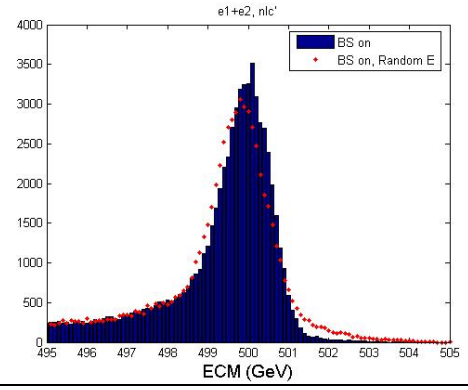	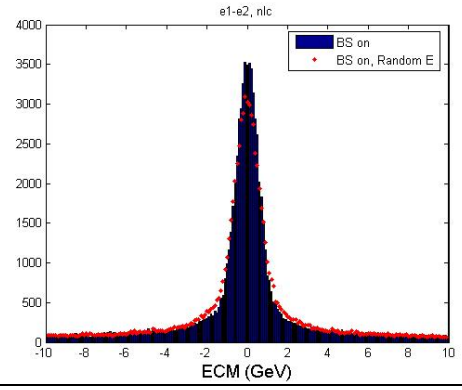

Figure 23 –E_1-E_2 and E_1+E_2 distributions for e^+e^- collisions for three LC parameter sets (NLC, TESLA, NLC′), comparing unaltered beams with beams with Energy-z correlations removed. The column on the left shows that there are significant differences in the luminosity spectrum when these correlations are removed. The column on the right shows, however, that there is no analogous change to the E_1-E_2 distribution—the distribution that is observable using the Bhabha acolinearity method.

4 Conclusion

When considering energy spread, but not initial state radiation or beamsstrahlung, a bias in the luminosity-weighted center-of-mass energy in e^+e^- collisions is found to be on the order of 50 ppm for TESLA parameters, 500 ppm for NLC parameters, and approximately 0 ppm for NLC'. The results are larger for e^-e^- collisions, with $E_{CM}^{bias}\Big|_{BSoff}$ on the order of 160 ppm for TESLA, 700 ppm for NLC, and -160 for NLC′. These result from the combined effect of finite energy spread, an Energy-z correlation, and a y-z kink instability.

When considering the additional effects of beamsstrahlung in e^+e^- interactions, the magnitude of the bias is increased by a factor of two for NLC and roughly threefold for TESLA, from enhanced head-tail luminosity variations (i.e. because the heads of the bunch collide with higher luminosity than the tails). It is also found that $E_{CM}^{bias}\Big|_{BSoff}$ and $E_{CM}^{bias}\Big|_{BSon}$ increase as the beams become more misaligned, i.e. in imperfect collisions.

We note that $E_{CM}^{bias}\Big|_{BSon}$ would be observable if Bhabha energies (E_1+E_2 distributions in Figure 23) could be accurately measured. However, it is unlikely that detector resolution and systematics are adequate for this[8,9]. One method proposed for determining the center-of-mass energy and luminosity spectrum is to use energy

spectrometer measurements of the incoming beam energies, together with Bhabha acolinearity measurements that effectively measure the (E_1-E_2) distribution of the colliding particles. But the $\boldsymbol{E}_{CM}^{bias}$ effects we have studied (resulting from the kink instability) cannot be determined from these experimental observables alone. In light of this, modeling of the beam-beam interaction and precise measurements of the incoming beam parameters are needed. Uncertainties in this modeling could limit the achievable precision in top or Higgs mass measurements. Fortunately, additional methods[13] of reconstructing the energy spectrum are being researched and seem promising: additional information from physics analyses of γZ, ZZ, WW, and μ-pair events will likely be necessary to extract the luminosity spectrum and luminosity-weighted E_{CM} to the desired precision.

References

[1] Woods, M., Moffeit, K.C., Raubenheimer, T, Seryi, A., Sramek, C, and Florimonte, A. – 2004 – *Luminosity, Energy, and Polarization Studies for the Linear Collider: Comparing e^+e^- and e^-e^- for NLC and TESLA*, SLAC-PUB-10353, IPBI TN-2004-1

[2] International Linear Collider Technical Review Committee – 2003 – *International Technical Review Committee Second Report*, SLAC-R-606

[3] Schulte, D., – 1998 – Ph.D. thesis (unpublished) – eConf C980914:127-131; also in *Monterey 1998, Computational accelerator physics*: 127-131

[4] Seryi, A. & Tenenbaum, P. – 2004 –*Alternative Main Linac BNS Configurations for Reduced Energy Spread* – SLAC-TN-04-042 and SLAC LCC Note 139

[5] Parameter Subcommittee of the International Linear Collider Steering Committee – 2003 – *Parameters for the Linear Collider* – Available from web site: http://www.fnal.gov/directorate/icfa/LC_parameters.pdf

[6] American Linear Collider Working Group – 2001 – *Linear Collider Physics Resource Book for Snowmass 2001* – SLAC-R-570

[7] Cinabro, D, Torrence, E., Woods, M. – 2003 – *Status of Linear Collider Beam Instrumentation Design* – SLAC ALCPG IPBI TN-2003-1

[8] Frary, M.N. & Miller, D.J. – 1991 – *Monitoring the Luminosity Spectrum** – DESY-92-123A:379

[9] Boogert, S.T., & Miller, D.J. – 2002 – *Questions about the Measurement of the e^+e^- luminosity Spectrum at a Future Linear Collider* – To appear in the proceedings of International Workshop on Linear Colliders (LCWS 2002), Jeju Island, Korea, 26-30 Aug 2002, hep-ex/0211021

[10] NLC Design Group – 1996 – *Zeroth-Order Design Report for the Next Linear Collider* – SLAC-474: Chapter 12

[11] Bower, G.R. & Cassell, R. – 2002 – *Linear Collider Detector Calorimetry*, SLAC-PUB-9479

[12] Frey, R. – 2001 – *Calorimeter Status and Possible Next Steps* – SLAC LCD Meeting September 18, 2001

[13] Hinze, A. – 2005 – *Determination of beam energy at TESLA using radiative return events* – LCnote LC-PHSM-2005-001

Appendices

A.1 acc.dat

acc.dat is the configuration file loaded by Guinea-Pig which contains the parameters of the accelerator being studied. The parameters are described in detail in the Guinea Pig User Manual[3]. In this study the parameters in the accelerator sections (NLC, TESLA) remained mostly consistent from run to run. The only factor that was consistently varied is the "charge sign", which is set to **-1** for electron-positron collisions and **+1** for electron-electron collisions. In the LC-GENERAL section, the general parameters for the simulation are established. This section contains the flags for energy spread ("do spread") and Beamsstrahlung ("do eloss"), which were altered to get the desired simulation. Also in this section, the variable "n_m", the number of macroparticles used in the simulation, was normally set to 15000 for NLC and 12000 for TESLA (corresponding to the number of particles in the input files used).

```
$ACCELERATOR:: NLC
{ energy     = 250 ;
  particles  = 0.75 ;
  sigma_x    = 243 ;
  sigma_y    = 3.0 ;
  sigma_z    = 110 ;
  emitt_x    = 3.6 ;
  emitt_y    = 0.04 ;
  espread    = 0.003 ;
  espread    = 0.003 ;
  which_espread = 3 ;
  charge_sign = -1 ;
  offset_y = 0. ;
}
```

```
$ACCELERATOR:: TESLA
{ energy     = 250 ;
  particles  = 2.00 ;
  sigma_x    = 553 ;
  sigma_y    = 5.0 ;
  sigma_z    = 300 ;
  emitt_x    = 10.0 ;
  emitt_y    = 0.03 ;
  espread.1  = 0.0014 ;
  espread.2  = 0.0007 ;
  which_espread = 3 ;
  charge_sign = -1;
}

$PARAMETERS:: LC-GENERAL
{ n_x=32 ;
  n_y=64 ;
  n_z=24 ;
  n_t=5 ;
  cut_x=3.0*sigma_x.1 ;
  cut_y=6.0*sigma_y.1 ;
  cut_z=3.0*sigma_z.1 ;
  n_m=12000 ;
  force_symmetric=0;
  integration_method=2 ;
  electron_ratio=1.0;
  ecm_min=2.0;
  load_beam= 3 ;
  do_eloss = 0 ;
  do_espread = 1 ;
  do_isr = 0 ;
  store_beam=1 ;
  do_photons=0 ;
  store_photons=0 ;
  do_pairs=0 ;
  do_compt = 0;
  do_hadrons=0 ;
  do_jets=0 ;
  do_lumi=1 ;
  num_lumi=40000 ;
  lumi_p=1e-29 ;
  do_lumi_ee_2=0;
  hist_ee_max=510.;
  hist_ee_bins=1020;
}
```

A.2 electron.ini and positron.ini

The input files *electron.ini* and *positron.ini* contain information about the incoming beams. Below is an example from *electron.ini*. Each element listed below was rounded an additional two decimal places in order to fit in this document.

```
2.49789e+002  3.25192e-001  4.33330e-003 -8.62750e+002  2.16795e+001 -9.22800e+000
2.50102e+002  2.60941e-001  5.36910e-003 -7.69187e+002 -3.85052e+001 -2.50427e+001
2.50232e+002  2.94785e-001 -1.02705e-003 -8.97431e+002  1.55385e+001 -3.04311e+000
2.49439e+002 -1.22069e-001 -4.60165e-003 -8.80835e+002  5.13209e+001 -8.76774e+000
2.49935e+002 -1.04828e-001  3.79758e-003 -7.44886e+002  5.63288e+001 -1.88497e+001
...
```

This file contains the following data:

col 1: particle energy
col 2: beam angle in x (radians)
col 3: beam angle in y (radians)
col 4: x-position at the intersection plane
col 5: y-position at the intersection plane
col 6: z-position (within the bunch)

A.3 beam1.dat

The output files *beam1.dat* and *beam2.dat* contain information about the outgoing beams. Following is an excerpt, a few lines from one of the files to demonstrate the format.

```
2.471654e+02 -4.086061e-05 -2.408405e-04 -3.249170e+02  6.132223e+01 2.065439e+01
2.472314e+02 -1.624232e-04 -2.018563e-04 -3.236250e+02 -1.289109e+02 9.045247e+00
2.470794e+02 -2.487935e-04 -2.444558e-04 -3.234080e+02 -8.365654e+01 2.937542e+01
2.471994e+02 -3.910802e-05 -2.446543e-04 -3.234050e+02  8.527923e+01 2.214249e+01
2.474644e+02  1.632229e-04 -1.818330e-04 -3.228530e+02  2.200606e+02 2.668889e+01
...
```

This file contains the following data:

col 1: particle energy
col 2: beam angle in x (radians)
col 3: beam angle in y (radians)

col 4: z-position (within the bunch)
col 5: x-position at the intersection plane
col 6: y-position at the intersection plane

A.4 lumi.ee.out

The file lumi.ee.out contains information about only the particles that created luminosity. A sample follows:

```
249.808  250.219 -286.948 -0.336367  72.0306
250.329  250.120  103.604 -1.019390  148.972
249.396  249.715  375.591 -4.860700  8.70473
249.444  249.589  129.005 -3.465230 -120.759
250.010  249.906 -188.921  0.735504 -13.3979
...
```

This file contains the following data:

col 1: energy of colliding electron
col 2: energy of colliding positron (or second electron in the case of e^-e^-)
col 3-5: x, y, z coordinates of the collision.

A.5 offsets and dispersion

I created two programs that enabled me to automate a large number of simulations, varying one parameter at a time. *offsets.m* and *dispersions.m* operated in a similar manner. The main components of the programs are as follows:

1) input user selections, including
    a. machine choice (NLC or TESLA)
    b. version of input file (electron#.ini and positron#.ini), where
    c. e^+e^- or e^-e^-
    d. offset type (y-offset, x-offset, y-waist-offset, x-waist-offset, y-dispersion, x-dispersion
    e. range of offset to scan and number of steps
2) start loop and run scans
    a. overwrite acc.dat based on the user input and the offset value being examined
    b. call *gp.exe*, the guinea pig simulation program

c. saving the relevant results before incrementing the loop variable and starting again

3) saving output
    a. data file is created
    b. graphs are generated
    c. option to save graphs to jpg

offsets.m is shown below in its entirety.

```
%================================================================
% Runs GP with varying x-, y-, x-waist-, and y-waist offsets
% Arik Florimonte
% 11 - 05 -03
%================================================================
clear all;
close all;
t_begin=cputime;
%WARNING: This program will overwrite acc.dat


acc = input('Enter accelerator parameter choice (NLC = 0, Tesla =
1): ');
if isempty(acc)
    error('invalid accelator');
end

efile = input('Enter electron/positron file set to use [1-25]: ');
if isempty(efile)
    error('No electron file selected');
end

%load electrons
switch acc
    case 0
        acc_name='NLC';
        lumi_max=2.5e34;
        n_m=15500.;
        sigma_x=243.;
        sigma_y=3.0;
        sigma_z=110.;
    case 1
        acc_name='TESLA';
        lumi_max=3.5e34;
        n_m=12000.;
        sigma_x=553.;
        sigma_y=5.0;
        sigma_z=300.;
    otherwise
        error('Invalid accelerator');
end
```

```
grid_size=1; % use scaling grid by default

% copy electron.ini and positron.ini files
if (efile >= 1) & (efile <= 99)
    file_cmd1 = strcat('copy /Y
.\',acc_name,'\electron',int2str(efile),'.ini electron.ini');
    file_cmd2 = strcat('copy /Y
.\',acc_name,'\positron',int2str(efile),'.ini positron.ini');
else
    error('invalid electron.ini or positron.ini file');
end
[ierr,result]=dos(file_cmd1);
[ierr,result]=dos(file_cmd2);

charge = input('Beam type? (0 = e+e-, 1 = e-e-) [e+e-] :');

if isempty(charge)
    charge = -1;
elseif isnumeric(charge)
    if charge==0
        charge=-1;
    else
        charge=1;
    end
else
    error('Invalid entry');
end

offs_type = input('Enter which offset to examine [0=y_offset,
1=y_waist, 2=x_offset, 3=x_waist] [0-3]: ');
if isempty(offs_type)
    error('Error: No value entered.');
end
switch offs_type
    case 0
        offset_rg = input ('Enter y_offset range in nm (i.e. -20 to
+20 is 40) [40]: ');
        if isempty(offset_rg)
            offset_rg=40;
        end
        if (offset_rg > 99) | (offset_rg < 1)
            offset_rg=40;
        end
    case 1
        offset_rg = input ('Enter y-waist offset range in um (i.e. -
2500 to +2500 is 5000) [5000]: ');
        if isempty(offset_rg)
            offset_rg=5000;
        end
        if (offset_rg > 9999) | (offset_rg < 1)
            offset_rg=5000;
```

```
        end
    case 2
        offset_rg = input ('Enter x_offset range in nm (i.e. -1000
to +1000 is 2000) [2000]: ');
        if isempty(offset_rg)
            offset_rg=2000;
        end
        if (offset_rg > 9999) | (offset_rg < 1)
            offset_rg=2000;
        end
    case 3
        offset_rg = input ('Enter x-waist offset range in um (i.e. -
200 to +200 is 400) [400]: ');
        if isempty(offset_rg)
            offset_rg=400;
        end
        if (offset_rg > 99999) | (offset_rg < 1)
            offset_rg=4000;
        end
    otherwise
        error ('invalid offset choice');
end

% loops = 9; %set number of steps
loops = input ('Enter number of loops to run [21]: ');
if isempty(loops)
    loops=21;
elseif (loops < 1) | (loops >101)
        loops=21;
end

if loops > 1 %make sure not dividing by zero
    offset_step = offset_rg/(loops-1);
else
    offset_step = 0;
end
offset_min= -round(offset_rg/2);

% initialize offset arrays
y_offset = zeros(1,loops);
y_waist = zeros(1,loops);
x_offset = zeros(1,loops);
x_waist = zeros(1,loops);

%set appropriate offset array to range of values
%also setup unique filename based on params
switch offs_type
    case 0
        for i=1:loops
            y_offset(i)=offset_min + (i-1) * offset_step; %set
y_offset value
        end
```

```
        datafn='yo';
        offs_nm='y-offset';
    case 1
        for i=1:loops
            y_waist(i)=offset_min + (i-1) * offset_step; %set
y_waist offset value
        end
        datafn='yw';
        offs_nm='y-waist';
    case 2
        for i=1:loops
            x_offset(i)=offset_min + (i-1) * offset_step; %set
x_offset value
        end
        datafn='xo';
        offs_nm='x-offset';
    case 3
        for i=1:loops
            x_waist(i)=offset_min + (i-1) * offset_step; %set
x_waist offset value
        end
        datafn='xw';
        offs_nm='x-waist';
end

pbeam=250.;

zero_gp_vars_sub; %zeros lumi, bpm_y1, bpm_y2, E_cm, std_E_cm,
rms_beam1

for i=1:loops
    acc_setup;
    gp_command=['guinea ' acc_name ' LC-GENERAL gp.out > gp.log'];
    [ierr,result]=dos(gp_command);
    [ierr,result]=dos(' read_gp_out < gp.out > gp_out.m');
    gp_out;

    load_gp_output_sub; %load gp output to our indexed variables
(lumi(i), bpm_y1(i), bpm_y2(i), bpm_x1(i), bpm_x2(i), rms_beam1(i)

    % load lumi data from lumi.ee.out
    lumi_data = load('lumi.ee.out');
    nlumi=length(lumi_data);
    i1=[1 0 0 0 0];
    i2=[0 1 0 0 0];
    e1_lumi=i1*lumi_data';
    e2_lumi=i2*lumi_data';
    E_cm(i)= (mean(e1_lumi+e2_lumi)-2*pbeam)/pbeam/2*1e6;
% mean ecm_lumi, in ppm
    std_E_cm(i) = std(e1_lumi+e2_lumi)/pbeam/2*1e6;
% 'std ecm_lumi'in ppm
end
```

```
if acc==1
    lumi = lumi.*1.41;
else
    lumi = lumi.*2.34;
end

%setup output format string
format_str='';
for i=1:loops
    format_str=strcat(format_str,'%16d\t');
end
format_str=strcat(format_str,'\n');

%finish setting up data file name
if (charge==-1)
    datafn=strcat(datafn,'(e+e-)');
else
    datafn=strcat(datafn,'(e-e-)');
end
datafn=strcat(datafn,lower(acc_name),int2str(offset_rg),'-
',int2str(loops),'file',int2str(efile),'.dat');
fid=fopen(datafn,'wb');
save_offs_data_sub; %writes offset scan data to file
fclose(fid);

%save data
c=fix(clock);
fid=fopen('offsets.log','ab');
fprintf(fid,'%s%s\n','Accelerator: ',acc_name);
fprintf(fid,'%s%s%d%s%d%s%d%s\n',offs_nm,' range from ',offset_min,'
to ',offset_min+((loops-1)*offset_step),' in ',loops,' steps');
fprintf(fid,'%s%s\n','Data saved to file: ',datafn);
fprintf(fid,'%s%s%s%d%s%d%s%d\n','Date: ',date,'; Time:
',c(4),':',c(5),':',c(6));
fprintf(fid,'%s%.2e%s\n\n','Elapsed time: ',cputime-t_begin,'
seconds');
fclose(fid);

%set offset = to the range of offsets we used
%setup x-axis label
switch offs_type
    case 0
        offset=y_offset;
        axis_lbl=strcat(offs_nm,' (nm)');
        angle1=bpm_y1;
        angle2=bpm_y2;
        y_lbl=' y-angle';
        prin_lbl='yoffset';
    case 1
        offset=y_waist;
        axis_lbl=strcat(offs_nm,' (um)');
```

```
        angle1=bpm_y1;
        angle2=bpm_y2;
        y_lbl=' y-angle';
        prin_lbl='ywaist';
    case 2
        offset=x_offset;
        axis_lbl=strcat(offs_nm,' (nm)');
        angle1=bpm_x1;
        angle2=bpm_x2;
        y_lbl=' x-angle';
        prin_lbl='xoffset';
    case 3
        offset=x_waist;
        axis_lbl=strcat(offs_nm,' (um)');
        angle1=bpm_x1;
        angle2=bpm_x2;
        y_lbl=' x-angle';
        prin_lbl='xwaist';
end


if charge == -1
    beam_2_nm='e+';
else
    beam_2_nm='e-';
end

graphttl=strcat(acc_name,' w/',beam_2_nm,'e- file:',int2str(efile));

plot_offsets_sub; %subroutine to graph offset data

prin=input('Print figures 1-4,6 to jpg? [y/n]: ','s');
if prin=='y'
    print_offsets_sub; %subroutine to print graphs to jpg
end
```

A.6 randomize_electron_E

The following subroutine is used to randomize the electron energy in the input file *electron.ini*, effectively removing any correlation between energy and z.

```
load electron.ini
load positron.ini

nevent=length(positron);
electron(:,1)=250*(1+sigma_E1*randn(nevent,1));
positron(:,1)=250*(1+sigma_E2*randn(nevent,1));

save -ascii electron.ini electron
save -ascii positron.ini positron
```

Bibiography

American Linear Collider Working Group – 2001 – *Linear Collider Physics Resource Book for Snowmass 2001* – SLAC-R-570

Boogert, S.T., & Miller, D.J. – 2002 – *Questions about the Measurement of the e^+e^- luminosity Spectrum at a Future Linear Collider* – To appear in the proceedings of International Workshop on Linear Colliders (LCWS 2002), Jeju Island, Korea, 26-30 Aug 2002, hep-ex/0211021

Bower, G.R. & Cassell, R. – 2002 – *Linear Collider Detector Calorimetry*, SLAC-PUB-9479

Cinabro, D, Torrence, E., Woods, M. – 2003 – *Status of Linear Collider Beam Instrumentation Design* – SLAC ALCPG IPBI TN-2003-1

Frary, M.N. & Miller, D.J. – 1991 – *Monitoring the Luminosity Spectrum** – DESY-92-123A:379

Frey, R. – 2001 – *Calorimeter Status and Possible Next Steps* – SLAC LCD Meeting September 18, 2001

Hinze, A. – 2005 – *Determination of beam energy at TESLA using radiative return events* – LCnote LC-PHSM-2005-001

International Linear Collider Technical Review Committee – 2003 – *International Technical Review Committee Second Report*, SLAC-R-606

NLC Design Group – 1996 – *Zeroth-Order Design Report for the Next Linear Collider* – SLAC-474: Chapter 12

Parameter Subcommittee of the International Linear Collider Steering Committee – 2003 – *Parameters for the Linear Collider* – Available from web site: http://www.fnal.gov/directorate/icfa/LC_parameters.pdf

Schulte, D., – 1998 – Ph.D. thesis (unpublished) – eConf C980914:127-131; also in *Monterey 1998, Computational accelerator physics* 127-131

Seryi, A. & Tenenbaum, P. – 2004 –*Alternative Main Linac BNS Configurations for Reduced Energy Spread* – SLAC-TN-04-042 and SLAC LCC Note 139

Woods, M., Moffeit, K.C., Raubenheimer, T, Seryi, A., Sramek, C, and Florimonte, A. – 2004 – *Luminosity, Energy, and Polarization Studies for the Linear Collider: Comparing e^+e^- and e^-e^- for NLC and TESLA*, SLAC-PUB-10353, IPBI TN-2004-1